

Are We Hungry for 3D LiDAR Data for Semantic Segmentation? A Survey and Experimental Study

Biao Gao, *Member, IEEE*, Yancheng Pan, *Member, IEEE*, Chengkun Li, *Member, IEEE*,
Sibo Geng, *Member, IEEE*, Huijing Zhao, *Member, IEEE*,

Abstract—3D semantic segmentation is a fundamental task for robotic and autonomous driving applications. Recent works have been focused on using deep learning techniques, whereas developing fine-annotated 3D LiDAR datasets is extremely labor intensive and requires professional skills. The performance limitation caused by insufficient datasets is called data hunger problem. This research provides a comprehensive survey and experimental study on the question: are we hungry for 3D LiDAR data for semantic segmentation? The studies are conducted at three levels. First, a broad review to the main 3D LiDAR datasets is conducted, followed by a statistical analysis on three representative datasets to gain an in-depth view on the datasets' size and diversity, which are the critical factors in learning deep models. Second, a systematic review to the state-of-the-art 3D semantic segmentation is conducted, followed by experiments and cross examinations of three representative deep learning methods to find out how the size and diversity of the datasets affect deep models' performance. Finally, a systematic survey to the existing efforts to solve the data hunger problem is conducted on both methodological and dataset's viewpoints, followed by an insightful discussion of remaining problems and open questions. To the best of our knowledge, this is the first work to analyze the data hunger problem for 3D semantic segmentation using deep learning techniques that are addressed in the literature review, statistical analysis, and cross-dataset and cross-algorithm experiments. We share findings and discussions, which may lead to potential topics in future works.

Index Terms—Data hunger, 3D LiDAR, semantic segmentation, deep learning

I. INTRODUCTION

TODAY, LiDAR has become the main sensor in many robotic [1] [2], mobile mapping [3] [4] and autonomous driving [5] [6] systems. 3D LiDAR data, captured from either a static viewpoint [7] or a mobile platform [8] during a dynamic procedure, provide a copy of the real world with rich 3D geometry in true size, which can be represented in the format of either 3D point clouds [9] [10] or 2D grids [11], e.g., range image, using a static or a sequence of data frames. Semantic segmentation [12] [13] is a fundamental task of scene understanding, which divides a whole piece of input data into different semantically interpretable categories according to a meaningful taxonomy in the real world. With the widespread use of LiDAR sensors in various applications, semantic segmentation of 3D LiDAR data [14] [15] is attracting increasing attention. Hereinafter, we refer to **3D semantic**

segmentation to emphasize the works addressing the features of 3D LiDAR data, and **semantic segmentation** for those of potentially general purpose.

Semantic segmentation has been studied for decades. A comprehensive review of early works up to 2014 is given in [16]. We refer to these works as **traditional methods**, which are characterized by using handcrafted features and bottom-up procedures. Inspired by the amazing success of deep learning techniques [17] [18], recent semantic segmentation works have focused on using deep neural networks to learn a richer feature representation, and model the mapping from input data to semantic labels in an end-to-end procedure [19], which are referred to as **deep learning methods** hereinafter. However, compared to traditional methods, deep learning methods face a considerable challenge of requiring large quantities of manually labeled data in training [20]. The quantity, quality and diversity of training data have a considerable influence on the generalization performance of deep learning models [21] [22].

The performance limitation caused by insufficient training data is called the **data hunger** effect, which is reflected on both data size and diversity. As noted by G.Marcus in [23], against the background of considerable progress and enthusiasm, the data hunger problem was his first concern among the ten challenges faced by the current deep learning systems. For 3D semantic segmentation tasks, 3D LiDAR data with point-wise annotation are required, where S3DIS [24], Semantic3D [7], and SemanticKITTI [8] are among the most popular datasets. These datasets are annotated fully or partially by human operators, which is time consuming, human intensive, and requires special skill and software, e.g., the operators are trained to handle professional software to visualize and annotate 3D point clouds, which are much harder to interpret than 2D images. Due to these difficulties, the publicly available datasets for 3D semantic segmentation are very limited in both data size and diversity compared with those of 2D images [25] [26]. Therefore, 3D semantic segmentation may face even severe data hunger problem.

In this research, we seek to answer the following questions. Are we hungry for 3D LiDAR data for semantic segmentation using deep learning techniques? Further, how serious is the problem on the aspect of both data size and diversity? What impact will the problem have on training deep 3D semantic segmentation models? What measures could be taken to solve the problem on the aspects of both methodology and dataset developing, and what are the remaining questions that need to be answered in future studies?

To answer the questions, the following steps are taken in this work. Section II reviews the existing 3D LiDAR datasets, and

B.Gao and Y.Pan are both the first authors of this paper. This work was supported in part by the National Natural Science Foundation of China under Grant 61973004 and in part by the Development Program of China under Grant 2017YFB1002601. B.Gao, Y.Pan, C.Li, S.Geng and H. Zhao are with the Key Lab of Machine Perception (MOE), Peking University, Beijing, China. Contact: H.Zhao, zhaohj@cis.pku.edu.cn.

through statistical analysis on three representative datasets, an in-depth view of data size and diversity is gained. Section III reviews the existing methods of 3D semantic segmentation, through which, three representative methods using deep learning methods are selected in Section IV, and experiments and cross examinations are conducted by training and testing on the datasets to find how datasets influence model performance. Section V reviews the efforts that have been conducted or potentially could be used to solve the data hunger problem of 3D semantic segmentation, followed by discussion on future topics and open questions in Section VI.

A number of surveys are relevant to this work. [27] [28] review early methods of 3D point cloud segmentation and classification in the literature. [12] [13] [29] review methods and datasets using for semantic segmentation. Furthermore, [30] [31] [14] [32] [15] [33] review the deep learning methods for 3D semantic segmentation task. In addition, [34] reviews multi-modal methods used for semantic segmentation and detection. However, these surveys focused on summarizing and classifying the existing methods, and none of them emphasize 3D datasets or the data hunger problem. To the best of our knowledge, this is the first work to provide an in-depth survey and experimental study on the data hunger problem for 3D semantic segmentation using deep learning techniques. The main contributions of our work are as follows:

- A broad review of the existing 3D datasets is provided that are divided into static, sequential and synthetic datasets according to the data acquisition methods and their main applications, and an organized survey of 3D semantic segmentation methods is given with a focus on the latest research trend using deep learning techniques.
- An in-depth view to the data hunger problem on the aspects of data size and diversity is gained through statistical analysis on three representative 3D datasets, and the impact of the problem on the performance of deep learning models is studied through experiments and cross examinations using three representative semantic segmentation methods.
- A systematic survey of the efforts to solve the data hunger problem is given on the aspects of both methodologies that require less on fine annotated data, and data annotation methods that are less labor intensive. An insightful discussion of remaining problems and open questions is given, leading to potential topics in future works.

II. 3D LiDAR DATASETS AND STATISTICAL ANALYSIS

Below, we review the publicly available 3D LiDAR datasets, followed by statistical analysis on three representative datasets.

A. 3D LiDAR Datasets

According to data acquisition methods and the main applications, 3D LiDAR datasets (as listed in Table I) are divided into three groups: 1) *Static datasets*: data collected from static viewpoints by terrestrial laser scanners or using MLS (Mobile Laser Scanning) systems that capture mainly static scene objects for applications such as street view, 3D modeling, and virtual realities. 2) *Sequential datasets*: data collected as sequences of frames from vehicular platforms for ADAS (Advanced Driving Assistance System) or autonomous driving applications, which can be further divided into datasets with point-wise or 3D bounding box annotations. 3) *Synthetic datasets*: data collected in a virtual world by simulating any of the above data acquisition systems. In addition, the most popular image and RGB-D datasets are also listed in Table I for comparison.

1) *Static datasets*: Static datasets are most commonly used for point cloud classification tasks. Their main application scenarios include robotics, augmented reality and urban planning.

As shown in Fig. 1(a), terrestrial laser scanners are usually used to collect static dense 3D LiDAR data from fixed viewpoints. MLS systems such as Fig. 1(b) capture sequences of LiDAR frames from a moving vehicle. However, the data are generally static which reconstruct a large-scale street view with no motion of dynamic objects.

2) *Sequential datasets*: Sequential datasets are most commonly used for autonomous driving tasks. As shown in Fig. 1(c), autonomous driving systems are exploited to capture the sequences of LiDAR frames with a moving viewpoint on the street. These datasets usually contain more frames but sparse points than static datasets. Besides, since the sensor's viewpoint moves along the direction of roads, the LiDAR points of road category usually distribute at certain angular regions, which can be predicted according to the system's setting.

Recent years, there appear sequential datasets with both point-wise and instance labels, which help research on 3D semantic segmentation [57] and panoptic segmentation [58].

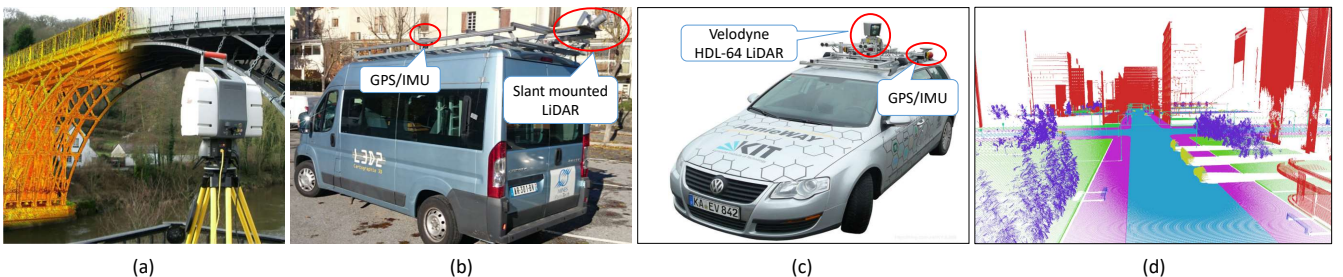


Fig. 1. Typical 3D LiDAR acquisition systems. (a) a terrestrial laser scanner, collects data from static viewpoints for *static datasets*, (b) a MLS (mobile laser scanning) system [35], collects data of mainly static scene objects for *static datasets*, (c) an autonomous driving system [36], collects 3D LiDAR streams for *sequential datasets*, (d) a simulation system [37] for *synthetic datasets*.

TABLE I
3D LIDAR DATASETS WITH COMPARISON TO REPRESENTATIVE IMAGE AND RGB-D ONES*

sensor	data type	anno.	dataset	frames	points/pixels	classes	scene ¹	ins.	seq.	sensor type ²	year	organization	license ³
3D LiDAR	static	point	Oakland [38]	17	1.6M	44	o	×	×	SL	2009	CMU	RO
			Paris-rue-Madame [39]	2	20M	17	o	✓	×	V32	2014	MINES ParisTech	ND-3.0
			TerraMobilita/IQmulus [40]	10	12M	15	o	✓	×	MLS	2015	Univ. of Paris-Est	ND-3.0
			S3DIS [24]	5	215M	12	i	×	×	MS	2016	Stanford Univ.	/
			TUM City Campus ⁴ [41]	631	41M	8	o	✓	✓	V64*2	2016	TUM	SA-4.0
			Semantic3D [7]	30	4009M	8	o	×	×	TLS	2017	ETH Zurich	SA-3.0
			Paris-lille-3D [35]	3	143M	50	o	✓	×	V32	2018	MINES ParisTech	ND-3.0
	sequential	point	Sydney Urban [42]	631	/	26	o	✓	✓	V64	2013	ACFR	/
			SemanticKITTI [8]	43552	4549M	28	o	✓	✓	V64	2019	Univ. of Bonn	SA-3.0
			SemanticPOSS [43]	2988	216M	14	o	✓	✓	HP	2020	Peking Univ.	SA-3.0
			A2D2 [44]	41277	1238M	38	o	✓	✓	V16*5	2020	Audi	ND-4.0
		3D-box	KITTI [36]	14999	1799M	8	o	✓	✓	V64	2012	KIT	SA-3.0
			H3D [45]	27K	/	8	o	✓	✓	V64	2019	HRI	RO
			nuScenes [46]	40K	2780M	23	o	✓	✓	U32	2019	nuTonomy	NC
			Lyft L5 [47]	46K	9936M	9	o	✓	✓	U64+U40*2	2019	Lyft Inc.	SA-4.0
			Argoverse [48]	22K	2354M	15	o	✓	✓	VV32*2	2019	Argo AI	SA-4.0
			Waymo [49]	230K	40710M	4	o	✓	✓	MR+SR*4	2020	Waymo LLC	Waymo Lic.
			A*3D [50]	39K	5093M	7	o	✓	✓	V64	2020	I2R	SA-4.0
			DENSE [51]	13.5K	/	4	o	✓	✓	V64	2020	Mercedes-Benz	NC
			synthetic	point	GTA-V [52]	/	/	/	o	×	✓	/	2018
SynthCity [37]	75000	367.9M			9	o	×	✓	/	2019	UCL	RO	
image/RGB-D	image	pixel	PASCAL VOC [25]	9993	/	20	i/o	×	×	Camera	2015	UoL/Microsoft	/
			Cityscapes [53]	24998	52425M	30	o	✓	✓	Camera	2016	Daimler	NC
	RGB-D	pixel	NYU-Depth V2 [54]	1449	445M	894	i	✓	✓	MK	2012	NYU	/
			ScanNet [55]	2500K	768000M	20	i	✓	✓	SS	2017	Stanford Univ.	RO
			ApolloScape ⁵ [56]	146997	1322973M	25	o	✓	✓	VUX*2	2018	Baidu Research	ApolloScape Lic.

* Abbreviation explanation. anno.: annotation, ins.:instance, seq.:sequential.

¹ **i** means indoor, **o** means outdoor

² **SL**: SICK LMS, **V32**: Velodyne HDL-32, **MLS**: Mobile Laser Scanner, **MS**: Matterport scanner, **V64**: Velodyne HDL-64E, **TLS**: Terrestrial laser scanner, **HP**: HESAI Pandora, **V16**: Velodyne VLP-16, **U32**: (unknown type) 32 channels LiDAR, **U64**: (unknown type) 64 channels LiDAR, **U40**: (unknown type) 40 channels LiDAR, **VV32**: Velodyne VLP-32, **MR**: Mid range LiDAR, **SR**: Short range LiDAR, **MK**: Microsoft Kinect, **SS**: Structure sensor, **VUX**: VUX-1HA laser scanner.

³ **ND-3.0**: CC-BY-NC-ND-3.0, **ND-4.0**: CC-BY-ND-4.0, **SA-3.0**: CC-BY-NC-SA-3.0, **SA-4.0**: CC-BY-NC-SA-4.0, **RO**: research only, **NC**: non-commercial

⁴ TUM City Campus dataset provides sequential LiDAR frames, but it was collected by a MLS system, so it is still categorized as a static dataset.

⁵ ApolloScape provides depth data only for static street views without moving objects.

3) *Synthetic datasets*: The generation of real datasets is extremely expensive due to the labor intensiveness of data annotation. Synthetic datasets are built through computer simulation, as shown in Fig. 1(d), which can be large scale and have fine but cheap annotations. The problem of using such datasets is caused by the large gap between synthetic and real scenes. Synthetic scenes can generally be very realistic, but they lack accuracy in detail. For example, pedestrians in the GTA-V [52] dataset have RGB information with rich details, but their physical models are simplified into cylinders, and the resultant point clouds lack the necessary details of real objects.

4) *Comparison with Image and RGB-D Datasets*: A few representative image and RGB-D datasets are listed in Table I, which have much larger scales. Comparing to image and RGB-D datasets, it can be found that whatever Cityscapes [53] and ApolloScape [56] for semantic segmentation in autonomous driving scenes, or ScanNet [55] for indoor scenes, their number of pixels/frames are more sufficient than 3D LiDAR ones. Although the studies on image and RGB-D still face the data hunger problem, it is more serious in the domain of 3D LiDAR datasets.

TABLE II
STATISTICAL ANALYSIS OF POINT/VOXEL PROPORTION WITH RESPECT TO RANGE DISTANCE OF 3D LIDAR DATASETS

	point proportion			
	< 10m	< 30m	< 50m	< 70m
Semantic3D	69.62%	90.12%	96.39%	99.52%
SemanticKITTI	62.54%	95.71%	99.94%	99.99%
SemanticPOSS	20.77%	78.42%	94.12%	98.91%
	voxel proportion			
	< 10m	< 30m	< 50m	< 70m
Semantic3D	4.56%	33.19%	65.37%	91.77%
SemanticKITTI	18.37%	74.39%	99.51%	99.92%
SemanticPOSS	5.41%	51.08%	82.01%	96.18%

* This table only considers points with labels and nonempty voxels.

B. Statistical Analysis of the Datasets

Three representative datasets are selected: 1) Semantic3D [7], the largest and most popular static dataset; 2) SemanticKITTI [8], the largest and most popular sequential dataset; and 3) SemanticPOSS [43], a new dataset that describes a dynamic urban scene with rich cars, people and riders. These datasets are analyzed statistically on the aspects of size and scene diversity.

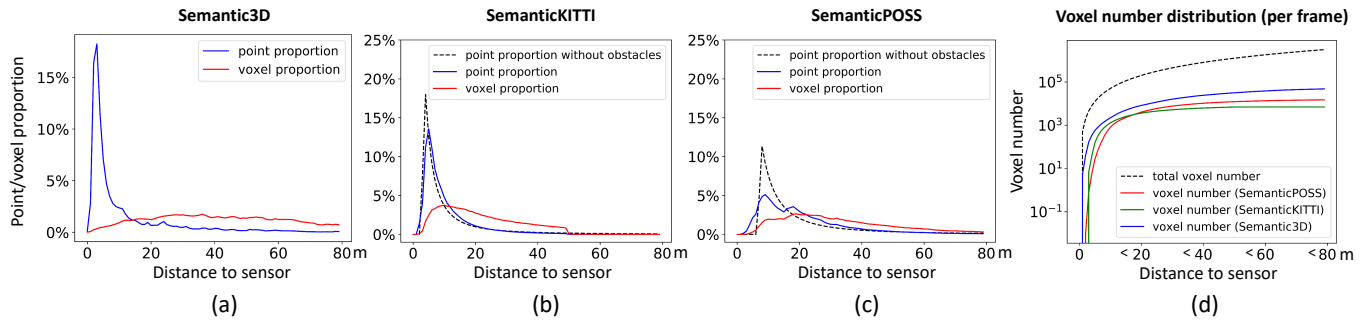


Fig. 2. Point/voxel proportion with respect to range distance: (a) Semantic3D (b) SemanticKITTI (c) SemanticPOSS, only LiDAR points with valid labels are counted. Point proportion without obstacles are simulated results for references. Semantic3D’s sensor settings are not public, so it is absent in (a). The problem of unbalanced spatial distribution of LiDAR points can be alleviated by voxelization. (d) voxel number distribution with respect to range distance. The difference between the curve “total voxel number” and others is the number of empty voxels for each dataset.

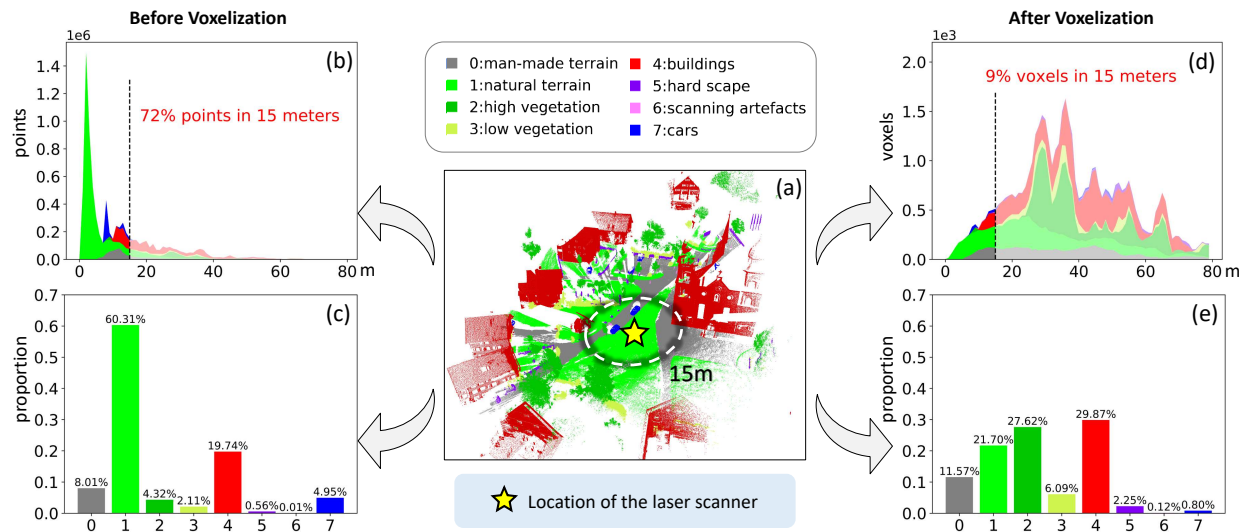


Fig. 3. Comparison of point/voxel proportion of a 3D LiDAR frame in Semantic3D. (a) Visualization of the 3D LiDAR frame. (b) Proportion of LiDAR points with respect to distance. (c) Proportion of LiDAR points with respect to categories. (d) Proportion of voxels with respect to distance. (e) Proportion of voxels with respect to categories. Voxels distribute more evenly and category proportion on voxels match more with the visualized scene.

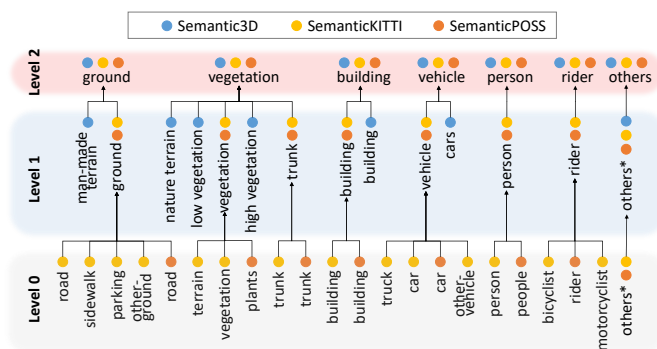


Fig. 4. Integration of the different label definitions of datasets. Level 0: some original labels of the datasets. Level 1: merged labels for per-dataset analysis. Level 2: merged labels for cross-dataset analysis. (*Some minor labels are merged as ‘others’ for simplicity.)

1) *Outline of the analysis:* A straightforward method for analyzing the dataset size is to count the point number and proportion. Table II and Fig. 2 show such statistics with respect to the range distance of three datasets as examples. It can be found that LiDAR points have a much higher density at near distances. For example, Semantic3D and SemanticKITTI

both have more than 60% of their LiDAR points measured within 10 m and less than 10% in [30m,70m]. SemanticPOSS is slightly different, as a LiDAR sensor (Pandora [59]) of unevenly arranged scan lines is used, which has a higher resolution on horizontal LiDAR scans. The spatial distribution of LiDAR points is very unbalanced in these datasets, which can be seen more visually in Fig. 3. Drawing a circle at 15m to the sensor’s location, 72% percent of the total 24,671,679 LiDAR points fall into the circle, where most are on a small section of natural terrain that has very similar properties.

This is a common phenomenon in current 3D LiDAR datasets, where close objects to the sensor’s location are measured with much higher point densities than farther ones. This fact causes it meaningless of counting point number directly, as large amount of points may bring few novel information and help little in model learning. On the other hand, the distribution of object categories is long-tailed. This is reflected in Fig. 3(b-c), for a dataset measured from an on-road viewpoint, large portion of data points could belong to *road*. Such long-tail problem could result in degraded performance of deep learning models on minority categories.

In this research, re-sampling of LiDAR points, **voxelization**,

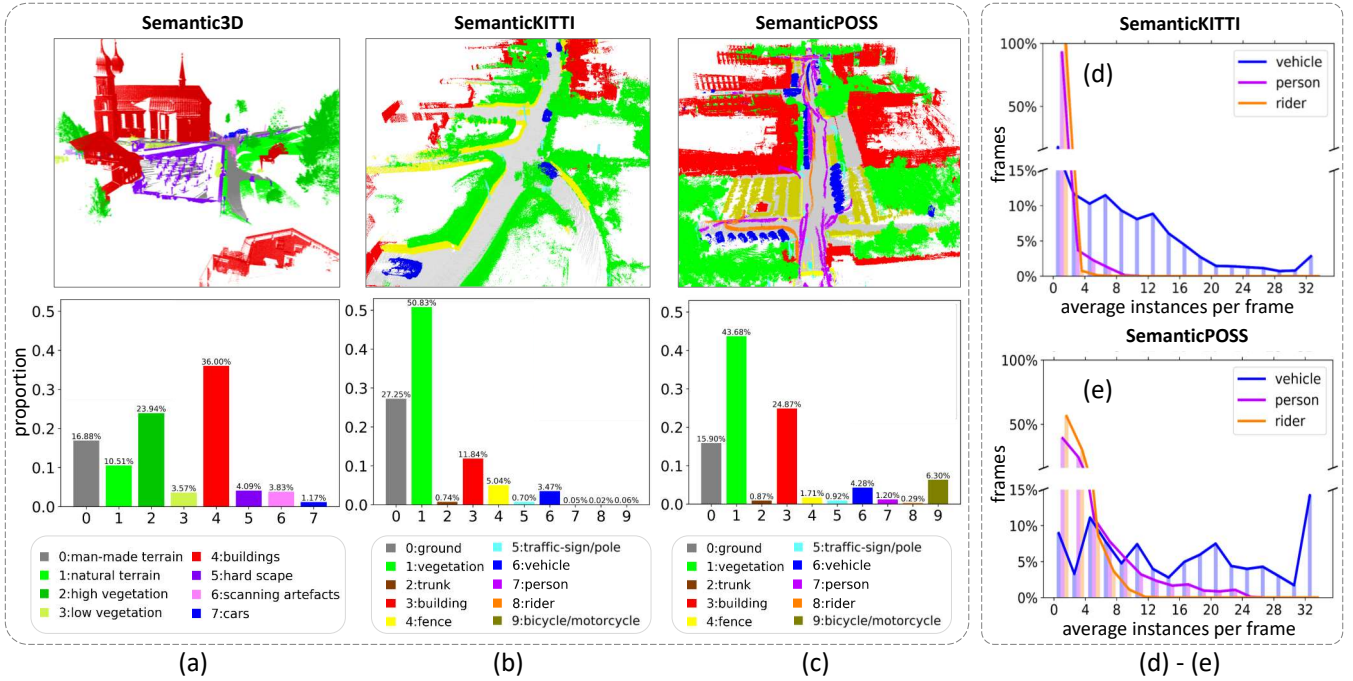


Fig. 5. Overall analysis of each dataset. (a-c) Each data set is visualized by a representative scene and a histogram of the scene descriptor of the whole dataset. (d-e) Per-frame average instance number of three kinds of dynamic objects. Semantic3D is absent since it describes mainly static scene and has no instance label.

is conducted to find datasets of uniform spatial resolution. Tessellating the 3D space evenly into voxels and projecting LiDAR points into the voxels, a set of valid voxels $V = \{v_i\}$ is obtained that has at least one LiDAR point in each, where v_i is a K -dimensional vector, with each column v_i^k denoting the proportion of LiDAR points of label k in the voxel i . In this research, a grid size is set of $(0.5\text{ m})^3$. It should be noted that in such a quantization process, the voxel values may vary with phase change. By counting the number and proportion of valid voxels, curves are plotted in Fig. 2(a-c), which show more even distributions with respect to distance. Similar results can also be found in Table II and Fig. 3. By the way, LiDARs can only scan the surfaces of obstacles, as a result, nonempty voxels actually occupy few space volume compared to total voxels of the whole scene (see Fig. 2(d)).

A number of measures are subsequently defined on voxels to analyze the statistics of the datasets. **Category proportion** \mathcal{C}^k is the proportion of LiDAR points or voxels having label k . **Scene descriptor** \mathcal{H} is a K -dimensional vector that characterizes the scene using category proportions. Given a voxel set V of a scene, a descriptor $\mathcal{H} = (\mathcal{C}^0, \mathcal{C}^1, \dots, \mathcal{C}^{K-1})$ is generated with each category proportion calculated as $\mathcal{C}^k = \sum_{v_i \in V} v_i^k / |V|$. In this research, V can be a voxel set of a single frame (Semantic3D), a sequence of frames (SemanticKITTI and SemanticPOSS) or a dataset. Given a **scene** \mathcal{S} , the scene descriptor is denoted as $\mathcal{H}_{\mathcal{S}}$. Usually, we use $\mathcal{H}_{\mathcal{S}}$ to represent the results on a single scene/sequence \mathcal{S} , and \mathcal{H} to represent the average results among the whole dataset. Dynamic objects such as vehicles, persons and riders have a much different nature than static objects such as buildings, trees and ground and are of special importance for autonomous driving applications. Thus, we define **dynamic scene descrip-**

tor \mathcal{O} , which is a vector of the dynamic categories only. The dynamic categories is a subset of \mathcal{H} 's category list, but each column of \mathcal{O} is the instance number of the category per frame. Similar with $\mathcal{H}_{\mathcal{S}}$, given a scene \mathcal{S} , the dynamic scene descriptor is denoted as $\mathcal{O}_{\mathcal{S}}$, and for a multiple frame scene, instance numbers are the per frame average. **Scene diversity distance** \mathcal{D} is used to measure the difference between two scenes on the scene descriptors. To balance the magnitude of different categories, we denote standardized scene descriptor $\tilde{\mathcal{H}}_{\mathcal{S}} = (\tilde{\mathcal{C}}^0, \tilde{\mathcal{C}}^1, \dots, \tilde{\mathcal{C}}^{K-1})$, where z-score standardized category proportion $\tilde{\mathcal{C}}^k = (\mathcal{C}^k - \text{mean}(\mathcal{C}^k)) / \text{std}(\mathcal{C}^k)$. Therein, the mean value $\text{mean}(\mathcal{C}^k)$ and standard deviation $\text{std}(\mathcal{C}^k)$ are calculated over all scenes of the three datasets. Given two scenes \mathcal{S}_i and \mathcal{S}_j , the scene diversity distance is estimated as $\mathcal{D}(\mathcal{S}_i, \mathcal{S}_j) = \|\tilde{\mathcal{H}}_i - \tilde{\mathcal{H}}_j\|_2 / K$. Similarly, **dynamic scene diversity distance** is defined as $\mathcal{D}_{\mathcal{O}}(\mathcal{S}_i, \mathcal{S}_j) = \|\tilde{\mathcal{O}}_i - \tilde{\mathcal{O}}_j\|_2 / K_{\mathcal{O}}$, in which $\tilde{\mathcal{O}}$ includes $\tilde{\mathcal{C}}^k$ of only dynamic categories and $K_{\mathcal{O}}$ is the number of dynamic categories. To balance the magnitude of different categories, standardization is also conducted on the values of category proportions to reduce dataset bias.

Each dataset has its own definition of labels/categories, which are much different. For comparison, merging of some labels is conducted as described in Fig. 4. **Level 0** is some original label definitions. Some labels with the same linguistic expression are not merged for their biased semantic context. For example, 'road' in SemanticPOSS includes sidewalk area, but excludes it in SemanticKITTI. **Level 1** is for per-dataset analysis, where moderately merge of some labels are conducted to keep the special characteristics of each dataset, while the results of different datasets can still be compared. **Level 2** is for cross-dataset analysis, where the labels are largely merged to find a uniform definition of the three datasets.

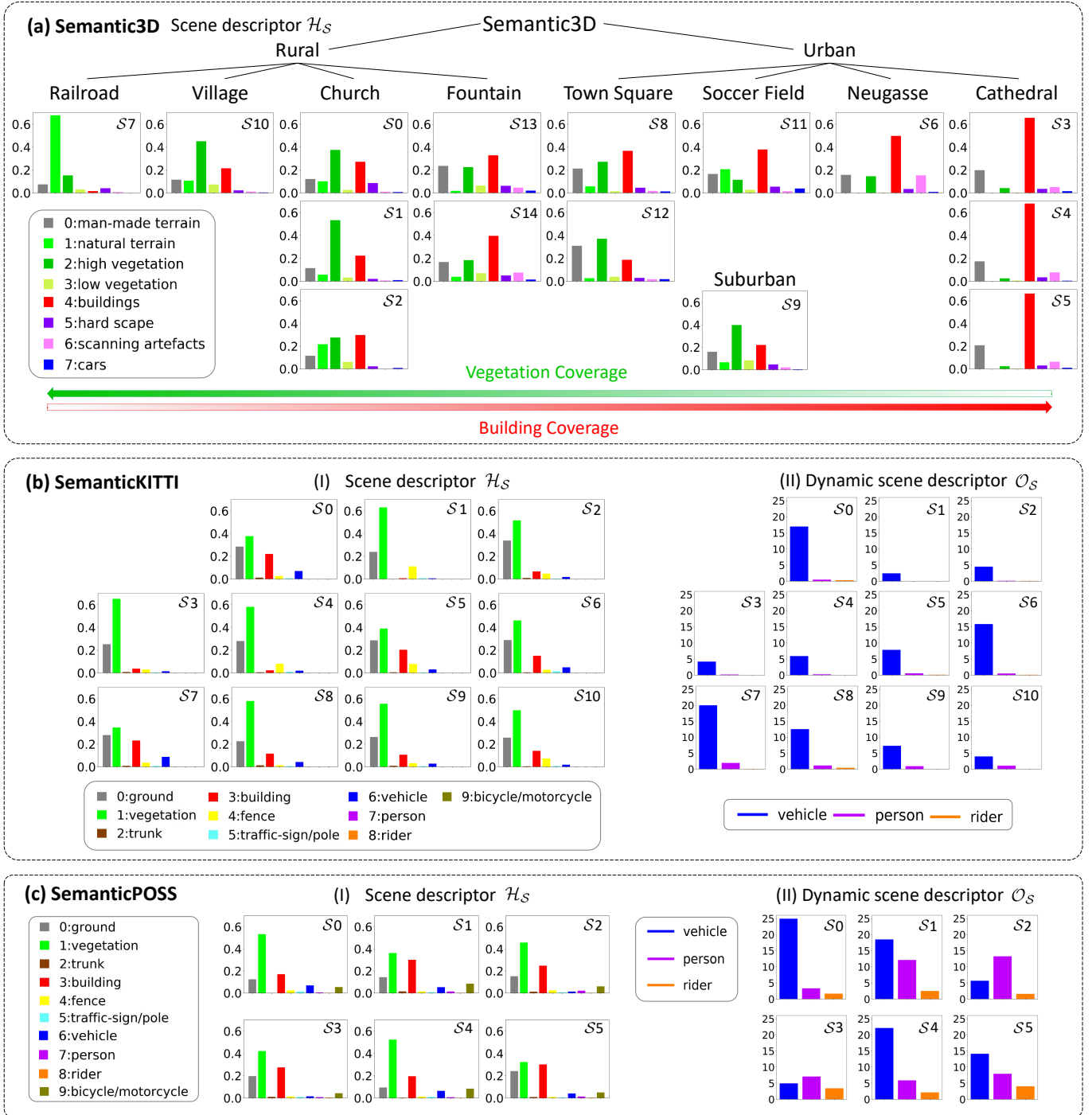


Fig. 6. Per-scene analysis of each dataset. (a) Scene descriptors of 15 Semantic3D scenes, each is one frame with dense LiDAR points. (b) (Dynamic) Scene descriptors of 11 SemanticKITTI scenes, each is a sequence of LiDAR frames. (c) (Dynamic) Scene descriptors of 6 SemanticPOSS scenes, each is a sequence of LiDAR frames.

Below, we first analyze each dataset on their features of scene description, then cross-scene and dataset comparison to statistically evaluate the difference in their scene diversity. Finally, we discuss the dataset concerning their representation of dynamic objects.

2) *Semantic3D*: Semantic3D contains 15 scenes in the training set. Each is a single frame that is measured using a terrestrial laser scanner from a fixed position. A scene is visualized in Fig. 5(a), with the whole dataset scene descriptor \mathcal{H} plotted as a histogram. It can be found that *ground*,

vegetation and *buildings* are the dominating categories, and the percentage of *buildings* is significantly higher than the other two datasets. It has no moving objects, except for a few parking cars.

The scenes of Semantic3D are divided into three groups, i.e., urban, rural and suburban according to the geographic location of the data measurement. As there is only one suburban scene S_9 , it is isolated from the tree structure in Fig. 6(a). Fig. 6(a) shows scene descriptor \mathcal{H}_S using histograms. It can be found that the \mathcal{H}_S of the same group could be very

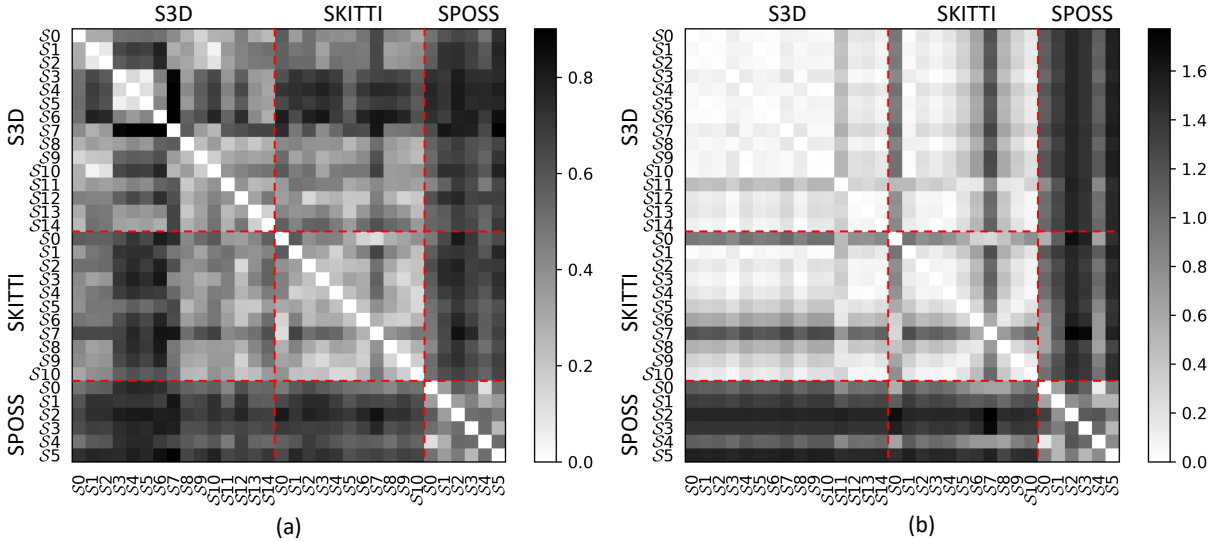


Fig. 7. Cross-dataset scene diversity distance analysis. Confusion matrixes of scene (a) and dynamic scene (b) diversity distance cross the scenes of three datasets. The darker the more difference of the scenes. (S3D: Semantic3D, SKITTI: SemanticKITTI, SPOSS: SemanticPOSS)

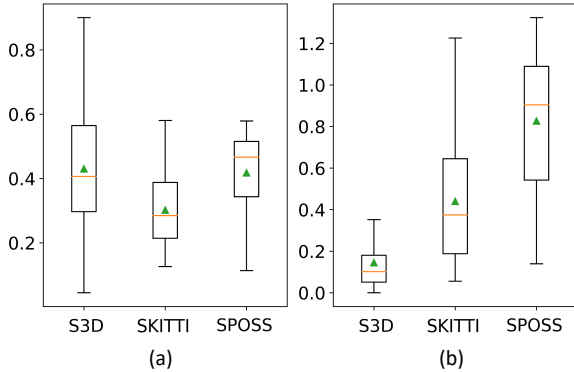


Fig. 8. Inner-dataset scene diversity distance analysis. Mean and variance of scene (a) and dynamic scene (b) diversity distance of each dataset, and their comparison. (S3D: Semantic3D, SKITTI: SemanticKITTI, SPOSS: SemanticPOSS)

different, e.g., \mathcal{S}_3 and \mathcal{S}_8 , whereas the scenes of different groups can be very similar, e.g., \mathcal{S}_8 and \mathcal{S}_{13} . Regardless of whether the scenes are in the same or different groups, the category proportions of scene objects are very diversified. For example, \mathcal{S}_7 is a railroad scene. It is full of natural terrain, with almost no buildings. \mathcal{S}_{3-5} are the opposite. They are cathedral scenes full of buildings but almost no vegetation.

Semantic3D has no moving objects such as *person* and *rider*. The dynamic scene descriptor \mathcal{O} is not adaptive to Semantic3D, and the corresponding results of Semantic3D are absent in Fig. 5 and Fig. 6.

In general, Semantic3D describes very diversified scenes. However, it describes static scenes with no moving object. Since each scene has only one LiDAR frame, this could create difficulty in training many deep learning methods.

3) *SemanticKITTI*: SemanticKITTI contains 11 sequences of 23, 201 LiDAR frames in training set that are measured continuously from a moving vehicle on European streets. Each sequence is treated in this research as one scene; therefore, 11 scenes are analyzed. One scene is visualized in Fig. 5(b), with the whole dataset scene descriptor \mathcal{H} plotted as

a histogram. Compared with Semantic3D, SemanticKITTI describes a wider street scene, where *vegetation* and *ground* are the two highest categories, possessing more than 50% and 27%, respectively. The proportion of *buildings* is low compared to other datasets.

SemanticKITTI provides instance labels of dynamic objects. The number of dynamic objects is an index to describe the complexity of a dynamic scene, which is analyzed by counting per frame instance number in Fig. 5(d). SemanticKITTI has a good diversity of *vehicle* distribution. However, *persons* and *riders* are scarce. Few scenes have more than 8 *persons* or 4 *riders*. This result is also confirmed by the dynamic scene descriptors \mathcal{O}_S of Fig. 6(b). From Fig. 6(b), the category proportions are not as diverse as Semantic3D.

The large data size makes SemanticKITTI very helpful for training deep learning models. However, the scenes are not as diversified as Semantic3D and have a limited number of dynamic objects.

4) *SemanticPOSS*: SemanticPOSS contains 6 sequences of LiDAR frames that were measured continuously from a moving vehicle on the campus of Peking University. Compared to the other 3D LiDAR datasets collected on structured roads or highways, SemanticPOSS describes scenes of abundant dynamic objects and mixed traffics.

Each sequence is treated as one scene; therefore, 6 scenes were analyzed. In Fig. 5(c), the whole dataset scene descriptor \mathcal{H} is plotted as a histogram, where a more dynamic street scene is described. From the scene descriptors of Fig. 6(c), its general scene diversity is generally similar to SemanticKITTI, but very different to Semantic3D.

The number of dynamic objects is analyzed in Fig. 5(e). Much wider distributions can be found, compared to SemanticKITTI, where the average instances per frame are distributed from 0 to 32 for the vehicle, 24 for the person and 12 for the rider. The dynamic scene descriptors \mathcal{O}_S of Fig. 6(c) confirms these results too, i.e., SemanticPOSS describes scenes populated by different kinds of dynamic objects and at

TABLE III
DYNAMIC SCENE OBJECTS WITH INSTANCE LABELS OF THE DATASETS

dataset	average instance per frame			category proportion (%)		
	vehicle	person	rider	vehicle	person	rider
Semantic3D	/	/	/	1.17	/	/
SemanticKITTI	10.09	0.63	0.18	3.47	0.05	0.02
SemanticPOSS	15.02	8.29	2.57	4.28	1.20	0.29

different crowded levels.

SemanticPOSS describes street scenes in a total of 2,998 LiDAR frames. The data size is limited with respect to SemanticKITTI, but it describes scenes of rich dynamics that are insufficient in other datasets.

5) *Cross-dataset Analysis*: A confusion matrix for scene diversity analysis is shown in Fig. 7(a), where each value is the scene diversity distance $\mathcal{D}(S_i, S_j)$ of the pair of scenes; the whiter the less diversity, and the darker the more diversity. For example, the first row compares the scene diversity distances of scene S_0 in Semantic3D with the others. Additionally, from Semantic3D, $\mathcal{D}(S_0, S_1)$ and $\mathcal{D}(S_0, S_2)$ are light gray, but $\mathcal{D}(S_0, S_3)$, $\mathcal{D}(S_0, S_4)$ and $\mathcal{D}(S_0, S_5)$ are much darker. The answer can be found in Fig. 6(a), where $S_{0,1,2}$ are rural churches, but $S_{3,4,5}$ are cathedral scenes. A similar confusion matrix is shown in Fig. 7(b) to analyze the dynamic scene diversity. Here, each value is the dynamic scene diversity distance $\mathcal{D}_O(S_i, S_j)$ of the pair of scenes.

The sub-matrices of datasets are visualized by boxplots in Fig. 8(a) for inner-dataset scene diversity analysis. Semantic3D has the lowest minimum and the highest maximum, reflecting richer inner-dataset scene diversity. SemanticPOSS generally has a higher median scene diversity.

In general, scenes from different datasets tend to be more diverse than those inner-dataset. The non-diagonal blocks in Fig. 7(a) are darker than diagonal blocks.

SemanticPOSS provides the richest dynamic scene diversity. Fig. 7(b) reflects the large dynamic scene difference between SemanticPOSS and the others. With values from the same dataset, three boxplots are drawn in Fig. 8(b). Because of the lack of moving objects in Semantic3D, its dynamic scene diversity is fairly low. From Table III, SemanticKITTI and SemanticPOSS both have many *vehicles*, where the average instances per frame are 10.09 and 15.02, respectively. In addition, SemanticPOSS has more instances of *person* and *rider*.

From the above analysis, we found that scenes could be very diverse that are not directly correlated with geographic location. The existing 3D LiDAR datasets reflect only a very small set of real world scenes, whereas they exhibit insufficient inner-dataset diversity, while large cross-dataset difference. One question is how these data sets help training deep learning models, and how the test results on these datasets provide useful guidance for real-world applications.

III. METHODS OF 3D SEMANTIC SEGMENTATION

In this section, we provide a brief and systematic review of the representative methods of 3D semantic segmentation.

A. Traditional and Deep Learning Methods

Methods of 3D semantic segmentation have been widely studied for decades. As illustrated in Fig. 9, they are divided into traditional and deep learning methods depending on feature representation and processing flow.

Traditional methods of 3D semantic segmentation often use handcrafted features to extract geometric information of points and output point labels from a classifier such as Support Vector Machine (SVM) or Random Forest (RF).

One common process of traditional methods is: over-segmenting point clouds followed by feature extraction and semantic classifiers. [60] and [61] [62] are representative methods using this process. The other common process is directly designing feature vectors of each point without prior over-segmentation, such as [63] and [64]. And on this basis, some methods [38] [61] [65] [66] use Conditional Random Fields (CRF) to aggregate contextual information.

Deep Learning Methods use deep neural networks to learn a feature representation and directly map input data to semantic labels through an end-to-end procedure. Recently, a number of studies on 3D LiDAR semantic segmentation have been developed using deep neural networks, which can be broadly divided into four groups, as illustrated in Fig. 9 according to the formats of input data: 1) point-based methods, 2) image-based methods, 3) voxel-based methods, and 4) graph-based methods. Below, we provide a more detailed review of these groups of methods.

B. Point-based Methods

Point-based methods take raw point cloud as input directly and output point-wise labels. These methods can process arbitrary unstructured point clouds. The main difficulty of raw point cloud processing is how to extract local contextual features from the unstructured point cloud.

1) *Point-wise Shared MLP*: PointNet [10] is the pioneer of point-based deep networks for unstructured point cloud processing. It uses shared Multi-Layer Perceptrons (MLP) to extract point-wise features and aggregates global features by symmetry max pooling operation. PointNet++ [67] improved PointNet [10] by introducing multi-scale grouping of neighboring points to extract local contextual features.

Inspired by PointNet++ [67], many methods seek improvements of local feature extraction in different ways, such as considering different definitions of 'neighbor' [68] [69] [70], using different sampling approaches [71] [57] [72], and designing specific layers [73] [74].

2) *Point Convolution*: Convolution is the core operation for feature extraction in 2D image semantic segmentation tasks, which requests ordered inputs for local contextual information extraction. Several methods contributed to constructing an ordered feature sequence from unordered 3D LiDAR data, and then convolutional deep networks were transferred to 3D LiDAR semantic segmentation. PointCNN [75] ordered K-nearest points by their spatial distance to the centers, which is called the χ -Conv operator for point convolution. In order to improve the convolution performance and efficiency, many

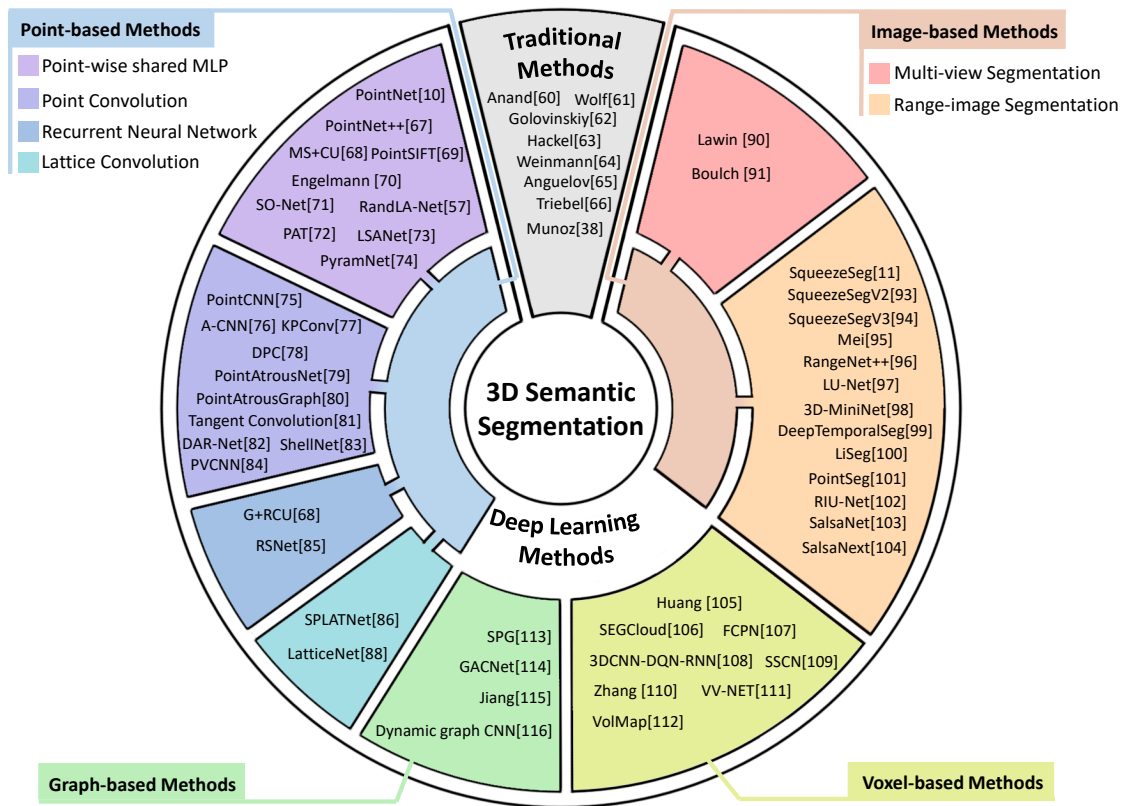


Fig. 9. Overview of 3D semantic segmentation methods.

specific convolutional networks were proposed, such as A-CNN [76], KPConv [77], DPC [78], PointAtrousNet [79], PointAtrousGraph [80], tangent convolution [81], DAR-Net [82], ShellNet [83], and PVCNN [84].

3) *Recurrent Neural Network*: Recurrent Neural Networks (RNN) are often used to extract contextual information of a sequence. For 3D semantic segmentation, RNN can extract spatial context by feeding ordered feature vectors in space. Engelmann et al. [68] proposed Grid (G) and Recurrent Consolidation Unit (RCU), which divide space into several grids as the network input. RSNet [85] transfers unordered points into an ordered sequence of feature vectors with a slice pooling layer. Then, RNN takes the sequence as input and aggregates spatial context information.

4) *Lattice Convolution*: A sparse permutohedral lattice is suitable for sparse data processing such as point clouds. SPLATNet [86] applies the Bilateral Convolution Layer (BCL) [87] to provide a transformation between point clouds and sparse lattices, which performs convolutions efficiently. And LatticeNet [88] introduced a novel slicing operator for lattice processing to obtain a better local feature representation.

C. Image-based Methods

Image-based methods project 3D LiDAR data onto a surface to generate 2D images as deep model inputs. These methods are usually derived from image semantic segmentation models, such as Fully Convolutional Network (FCN) [19] and U-Net [89]. The output predictions with pixel-wise labels are reprojected to origin 3D LiDAR points.

1) *Multi-view Segmentation*: A simple projection strategy is choosing several positions for taking photos of given point clouds. Lawin et al. [90] rotated a virtual camera around a fixed vertical axis to generate multi-view synthetic images, which were processed by a FCN-based multi-stream architecture. Boulch et al. [91] generated a mesh of 3D LiDAR data, and then produced images by randomly choosing virtual camera positions. For these multi-view methods, it is important to choose appropriate camera positions and projection strategies to reduce information loss.

2) *Range Image Segmentation*: Range images are usually generated by projecting one frame of 3D LiDAR data onto a spherical surface. SqueezeSeg [11] is a typical end-to-end network for range image semantic segmentation based on SqueezeNet [92] and CRF. SqueezeSegV2 [93] and SqueezeSegV3 [94] are improved versions of SqueezeSeg.

Range image segmentation methods are usually implemented on sequential datasets, while spatial and temporal information can be incorporated. Mei et al. [95] and RangeNet++ [96] introduced spatial constraints for predictions with more region consistency. LU-Net [97] and 3D-MiniNet [98] introduced 3D spatial features to the projected range images. DeepTemporalSeg [99] introduced temporal constraints based on a Bayes filter to make predictions more temporally consistent.

Some range image segmentation methods have focused on real-time performance, which is essential for applications such as autonomous driving and unmanned detectors, such as LiSeg [100], PointSeg [101], RIU-Net [102], SalsaNet [103] and

SalsaNext [104].

D. Voxel-based Methods

Voxel-based methods transfer 3D LiDAR data into voxels for structured data representation. These methods usually take voxels as input and predict each voxel with one semantic label.

A number of voxel-based methods [105] [106] [107] are based on 3D Convolutional Neural Network (3D CNN). However, it is challenging for voxel-based methods to find a proper voxel size that balances precision and computational efficiency. Some methods have contributed to reducing computational cost of 3D convolution on sparse data while maintaining acceptable accuracy, such as 3DCNN-DQN-RNN [108], Submanifold Sparse Convolution [109], efficient convolution [110], VV-NET [111], and VolMap [112].

E. Graph-based Methods

Graph-based methods construct a graph from 3D LiDAR data. A vertex usually represents a point or a group of points, and edges represent adjacency relationships between vertices. Graph construction and graph convolution are two key operations of these methods.

Super-Point Graph (SPG) [113] is a representative work. This network employs a PointNet [10] to encode vertex features and graph convolutions to extract contextual information. GACNet [114] proposed a novel graph convolution operation, Graph Attention Convolution (GAC), to consider structural relations between points of the same object. In order to learn more valid local features, some methods [115] [116] try to construct graph dynamically instead of fixed graph.

IV. DATA HUNGRY OR NOT? EXPERIMENTS

As addressed in the previous sections, three representative datasets, Semantic3D [7], SemanticKITTI [8] and SemanticPOSS [43], are analyzed statistically. In this section, we design three experiments to answer the following questions: How do scene diversity and training dataset size influence the model performance? Does the data hunger problem in scene diversity and dataset size exist for 3D LiDAR datasets? Do different models have different sensitivity to the data hunger effect?

More specifically, as reviewed in previous section, 3D semantic segmentation methods using deep learning techniques can be broadly divided into four groups according to their input data format. The experiments below explore whether the models of different input data formats face different degree of data hunger.

A. Selected Methods in Experiments

Three methods are selected in the experiments, PointNet++ [67], SqueezeSegV2 [93], and SPG [113], representing the fundamental architectures of point-, image- and graph-based methods respectively, which are of broad awareness. Since voxel-based method share the features of both point- and image-based ones, it is absent in this experiment.

PointNet++ is a typical point-based method taking raw point clouds as input. PointNet++ is a hierarchical encode-decode structure based on shared MLP. The sampling, grouping, and PointNet layer are used to learn local contextual features. Many point-based methods are derived from the PointNet++ architecture.

SqueezeSegV2 is a typical image-based method taking range images as input. The architecture of SqueezeSegV2 is a typical convolutional neural network. It is chosen as a deputy

TABLE IV
DESIGN OF EXPERIMENTS.

	Experiment 1 cross-scene generalization evaluation.	Experiment 2 cross-dataset generalization evaluation.	Experiment 3 Dataset size effects evaluation.
Scope	Scene diversity	Scene diversity	Dataset size
Purpose	Train models on a single dataset with different scene diversity, and examine how the data hunger problem of scene diversity affects models' performances.	Train models on different datasets, and examine how the data hunger problem of scene diversity affects models' performances.	Examine how the data hunger problem of dataset size affects models' performances, and whether the models are hungry for dataset size.
Dataset	Semantic3D	SemanticKITTI, SemanticPOSS	SemanticKITTI
Model	PointNet++, SPG	PointNet++, SqueezeSegV2, SPG	PointNet++, SqueezeSegV2, SPG
Method	Three sub-datasets are made on Semantic3D, 1) urban: a dataset contains urban scene only, 2) rural: a dataset contains rural scenes only, 3) mix: a dataset contains both rural and urban scenes. Each sub-dataset is divided randomly into two parts for training and testing. The selected models are trained and tested crosswise on these sub-datasets.	Three datasets are used, SemanticKITTI, SemanticPOSS, and a mixed dataset, which contains both SemanticKITTI and SemanticPOSS data. Similar to Experiment 1, selected methods are trained and tested crosswise on these datasets.	Evaluate the model performance using different amounts of training data. We use parts of SemanticKITTI data to train the models and compare mIoU of the model predictions.
Label for testing	<i>man-made terrain, natural terrain, high vegetation, low vegetation, building, hard scape, car</i>	<i>person, rider, vehicle, traffic sign/pole, trunk, vegetation, fence, building, bicycle/motorcycle, ground</i>	<i>person, rider, vehicle, traffic sign/pole, trunk, vegetation, fence, building, bicycle/motorcycle, ground</i>
Other details	Weights of all categories are the same for training.	Weights of all categories are the same for training. Single frame of point clouds is used as input, not overlapped frames.	Weights of all categories are the same for training. Single frame of point clouds is used as input, not overlapped frames.
Result	Table V, Fig. 10(a)	Table VI, Fig. 10(b)	Table VII, Fig. 11(a)

TABLE V
RESULT OF EXPERIMENT 1: CROSS-SCENE GENERATION EVALUATION.

Category	Model	PointNet++			SPG		
		Test	Train		urban	rural	mix
man-made terrain	urban	95.3	90.0	94.3	99.7	99.6	99.6
	rural	89.0	91.8	88.3	80.0	96.1	96.5
	mix	92.2	90.5	91.4	97.7	99.3	99.4
natural terrain	urban	92.1	68.0	85.6	93.8	79.3	84.6
	rural	80.0	85.3	78.3	32.8	92.4	91.1
	mix	82.1	79.3	79.6	51.2	88.1	89.1
high vegetation	urban	88.5	91.3	90.9	91.4	93.2	93.4
	rural	90.2	93.3	87.4	11.2	85.9	34.7
	mix	90.2	93.1	88.1	49.0	89.1	60.8
building	urban	96.5	95.9	97.5	95.3	87.3	94.1
	rural	89.8	92.3	88.5	76.9	95.1	92.8
	mix	94.0	94.5	93.9	90.7	88.9	93.8
mIoU	urban	69.6	62.0	68.6	80.5	68.4	78.9
	rural	71.9	78.9	73.5	38.3	86.6	71.4
	mix	71.7	72.1	71.7	62.6	75.3	75.7

¹ IoU of some dominant categories. Deeper color means the better performance on a specific test scene using a model.

of CNN-based architectures, which is similar to most image-based methods.

SPG is a typical graph-based method taking the super-point graph as input. A segmentation algorithm is used to partition point clouds into several groups as vertexes of the graph. Edges are constructed to represent contextual relationships between vertexes by comparing the shape and size of the adjacent point groups. The PointNet layer and Gated Recurrent Unit (GRU) are used to learn local contextual features and implement graph convolution.

B. Outline of the Experiments

For the 3D semantic segmentation task, deep learning models need to give semantic predictions to every point of the given point cloud. To evaluate the model performance, we use the Intersection over Union (IoU) given by

$$IoU_c = \frac{TP_c}{TP_c + FP_c + FN_c} \quad (1)$$

where TP_c, FP_c, FN_c denote the number of true positive, false positive, false negative predictions of category c . Let N be the number of categories used for measurement, the mean IoU (mIoU) is defined as the arithmetic mean of IoU, namely,

$$mIoU = \frac{1}{N} \sum_{c=1}^N IoU_c \quad (2)$$

To analyze the data hunger effect of scene diversity and data size, three experiments shown in Table IV, are designed.

C. Results

The results of Experiment 1,2 are shown in Table V and Table VI. Because SemanticKITTI is much larger than SemanticPOSS, we add different weights when calculating the

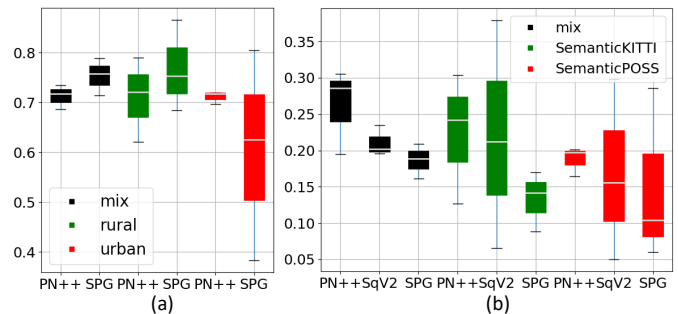


Fig. 10. mIoU of the models trained on different scenes (PN++: PointNet++, SqV2: SqueezeSegV2). (a) Result of Experiment 1. (b) Result of Experiment 2. The different color of box means different training scenes. The values of vertical axis means mIoU. Each box shows the maximum, minimum and median of the mIoU on different test set.

mIoU of the mixed dataset to balance the data size bias. The IoU of the mixed dataset is given by

$$IoU_{mix} = \frac{w_{SK} \cdot TP_{SK} + w_{SP} \cdot TP_{SP}}{w_{SK} (|SK| - TN_{SK}) + w_{SP} (|SP| - TN_{SP})} \quad (3)$$

where TP_{SK}, TN_{SK} denote the number of true positive, true negative predictions of SemanticKITTI data, and $|SK|, |SP|$ denote the number of LiDAR scans of SemanticKITTI and SemanticPOSS. The weights are inversely proportional to the dataset size.

$$w_{SK} = \frac{|SP|}{|SK| + |SP|}, w_{SP} = \frac{|SK|}{|SK| + |SP|} \quad (4)$$

In Table V and Table VI, experimental performances are colored in units of 3×3 blocks. In each 3×3 block, the best result in each row is marked as the deepest red, and the worst is white. The medium results are colored depending on their distance to the best one. Let us see the left bottom 3×3 block in Table V as an example, i.e., mIoU of different models based on PointNet++. In the first row, 69.6 indicates that the model trained on the urban set performs the best on the urban test set, and the model trained on the rural set achieves the worst mIoU (62.0) on the urban test set. For both Table V and Table VI, we can see a specific model's performance on different test scenes from a column view, and the performances of different models on a specific test scene from a row view.

To compare the general performance and robustness of a specific model, we use the box plot shown in Fig. 10. Each box shows the maximum, minimum and median of the mIoU on different test sets. A higher position of a box indicates that the model performs relatively better, and a shorter length of a box indicates that the model performs relatively robustly.

The results of Experiment 3 are shown in Table VII and Fig. 11(a). The curve of Fig. 11(a) shows the performance trends of the models changing along with the training data size.

D. Discussions

We will answer the question of whether deep learning methods are data hungry for 3D semantic segmentation from two aspects, scene diversity and dataset size.

TABLE VI
RESULT OF EXPERIMENT 2: CROSS-DATASET GENERATION EVALUATION.

Category	Model	PointNet++			SqueezeSegV2			SPG		
		Test	Train		SKITTI	SPOSS	mix	SKITTI	SPOSS	mix
person	SKITTI	0.7	6.4	1.8	15.4	2.9	5.7	2.8	0.9	3.9
	SPOSS	0.0	20.8	18.7	0.0	18.4	15.8	4.2	17.2	18.0
	mix	0.0	18.2	17.4	2.6	16.9	14.5	4.0	9.1	17.4
vehicle	SKITTI	53.2	16.6	53.1	68.5	8.0	30.1	49.0	15.9	46.2
	SPOSS	4.1	8.9	8.8	1.6	34.9	15.7	15.3	11.5	14.3
	mix	44.7	17.4	42.5	57.3	8.6	27.5	42.1	15.3	39.6
vegetation	SKITTI	64.0	48.2	64.3	79.9	0.2	40.0	51.2	33.8	51.7
	SPOSS	46.3	51.2	50.0	8.9	56.3	22.7	49.2	52.8	52.4
	mix	56.3	49.7	58.4	53.9	22.2	34.6	50.4	40.2	52.0
building	SKITTI	61.8	41.5	62.7	69.7	9.6	47.1	38.7	16.2	33.7
	SPOSS	18.9	42.7	36.7	9.2	47.0	47.0	34.3	55.3	51.6
	mix	40.3	42.0	49.2	37.9	27.3	47.1	36.7	33.7	42.6
ground	SKITTI	80.9	57.2	80.8	88.5	28.9	66.3	51.3	36.8	51.4
	SPOSS	40.0	62.2	62.0	45.1	71.3	56.5	36.3	75.6	73.4
	mix	68.6	58.8	75.0	70.4	41.7	63.5	46.2	48.8	58.8
mIoU	SKITTI	30.4	16.4	30.5	37.9	5.0	23.5	17.0	6.0	16.1
	SPOSS	12.7	20.1	19.5	6.6	29.8	19.6	8.8	28.6	20.9
	mix	24.2	19.7	28.6	21.2	15.6	20.2	14.2	10.4	18.9

¹ SKITTI denotes SemanticKITTI, SPOSS denotes SemanticPOSS.

² IoU of some dominant categories. Deeper color means the better performance on a specific test scene using a model.

1) *Scene diversity*: From the results of Experiment 1 and Experiment 2, we can summarize our findings as follows:

- **Performance decrease occurs when testing a model at scenes much different from the training scenes.** As shown in Table V, all models trained on rural scenes have a performance decrease when testing on urban scenes, and vice versa. This is probably caused by the high scene diversity between urban and rural scenes. A similar phenomenon appears in experiments with SemanticKITTI and SemanticPOSS, as shown in Table VI. Apart from the mixed dataset, mIoU always decreases when testing on different datasets with the training dataset. Both Table V and Table VI show deeper color on the diagonal of each 3×3 block, which indicates better performance on similar scenes.

- **Preponderant categories are easier to distinguish.** A specific example is the *high vegetation* in Table V. Models trained on rural scenes are good at classifying *high vegetation* because of its preponderance in rural scenes. Table VI shows a similar phenomenon. For example, SemanticPOSS has a higher density of *person* than SemanticKITTI but fewer samples of other categories. As a result, models trained on SemanticPOSS achieve better performance on *person*, but are generally weaker on other categories.

- **High scene diversity of a training set can improve the robustness of the model.** As shown in Table V and Table VI, models training on the mixed scenes obtain acceptable predictions regardless of the test scenes. Fig. 10 summarizes different model performances using boxplots. Obviously, the mixed model has shorter boxes, which means a narrow distribution of minimum/maximum mIoU in general, showing its more stable performance and robustness.

- **Mixing multiple datasets in training may not improve**

model performance. On the other hand, through Table V and Table VI we can find that the performances of models training on the mixed scenes are not the best on most test scenes. Simply merging more datasets to obtain better scene diversity will face great resistance, and even lead to model performance decreases due to the large domain gap between datasets, which are further discussed in Section VI.

- **In summary, the data hunger problem in scene diversity currently exists for 3D LiDAR datasets.** Lack of some specific category or biased category distribution are common phenomena for datasets. For example, Semantic3D does not have dynamic categories such as *person*, making it unsuitable for applications such as autonomous driving systems. And a single dataset usually does not have enough scene diversity to obtain a well-generalized model. Furthermore, some other factors also affect model performance, such as the sensor difference. The image-based approaches suffer from this effect because of the difference in vertical resolution, as we can find SqueezeSegV2 performances drop more drastically while testing on another dataset in Table VI. Therefore, the data hunger problem in scene diversity is still challenging for 3D LiDAR semantic segmentation models to improve their generalization ability.

2) *Dataset size*: The results of Experiment 3 illustrate the facts as follows:

- **Increasing training data improves model performance.** All three models show uptrends with increasing training data. It is easy to understand that incremental data provides more features and information for models.

Second, different models have different sensitivities to the quantity of training data. As shown in Fig. 11(a), the uptrend of SqueezeSegV2 is more significant than that of

TABLE VII
RESULT OF EXPERIMENT 3 – DATASET SIZE EFFECTS EVALUATION.

Category	size		12.50%	25%	50%	75%	100%
	Model						
person	PointNet++		0.3	0.3	0.4	0.5	0.7
	SPG		0.6	0.4	1.1	1.0	2.3
	SqueezeSegV2		1.3	3.0	6.9	7.5	15.4
vehicle	PointNet++		52.2	54.4	54.5	54.5	54.9
	SPG		44.9	46.2	47.0	48.8	50.1
	SqueezeSegV2		61.6	68.4	71.6	74.7	78.4
vegetation	PointNet++		63.3	64.7	64.1	62.8	64.0
	SPG		47.4	47.9	53.1	52.6	52.7
	SqueezeSegV2		60.2	66.6	70.8	71.7	72.6
building	PointNet++		59.2	61.7	61.8	60.6	61.9
	SPG		33.2	36.7	34.1	36.1	38.0
	SqueezeSegV2		57.6	64.7	68.4	69.0	69.7
ground	PointNet++		63.0	63.5	64.4	65.0	65.3
	SPG		45.0	44.9	50.7	51.9	52.2
	SqueezeSegV2		78.7	79.7	86.2	88.2	88.2
mIoU	PointNet++		27.6	29.7	30.0	30.1	30.4
	SPG		13.2	14.5	15.2	15.8	17.1
	SqueezeSegV2		24.4	28.2	32.6	34.5	37.2

¹ IoU of some dominant categories using different training dataset size. Experiment on SemanticKITTI dataset.

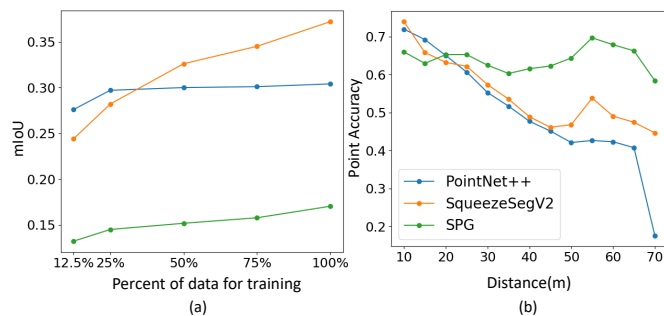


Fig. 11. (a) Plots of training DATASET SIZE v.s. MODELS IoU. Experiment on SemanticKITTI dataset. (b) Plots of MODELS accuracy with respect to distance. Experiment on SemanticPOSS dataset.

PointNet++. It seems that the data requirements of different models are different. SqueezeSegV2 takes range images as input, which are sensitive to the LiDAR’s position. Incremental LiDAR frames in a scene captured at different viewpoints may provide more information for range image inputs than point cloud inputs. Therefore, the curve of PointNet++ seems to be saturated with 25% training data, while the curve of SqueezeSegV2 maintains its growing trend.

- **In summary, the data hunger problem for dataset size exists for current 3D LiDAR datasets.** The continuous uptrend of the mIoU-size curve indicates that the model does not reach limit of its ability and requires more data for improvement. It can be predicted that the mIoU will continue increasing if more training data are used. All three models show a continuous uptrend to different degrees when adding training data. Therefore, for most deep learning models, existing datasets are not sufficient.

3) *Instance Distance and Quality*: In 3D datasets, point clouds become sparser with increasing distance to the sensor. Therefore, the points far away from the sensor are hard to be correctly classified. As shown in Fig. 11(b), the model

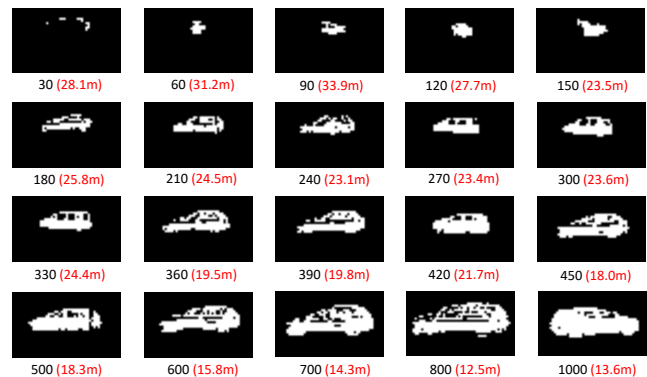


Fig. 12. Car instances with different point number in range image. The point numbers of instances are shown in black text and corresponding distances are shown in red text.

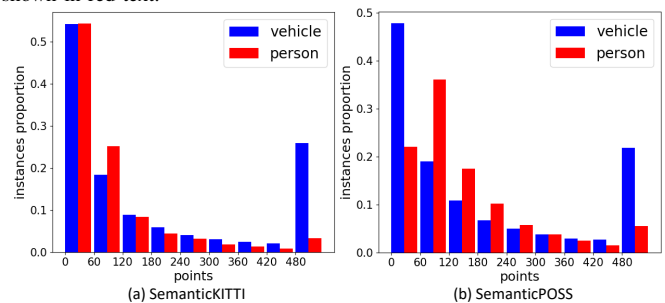


Fig. 13. Instances with different point number distribution in SemanticKITTI and SemanticPOSS.

prediction accuracy decreases with increasing distance, but their downtrends are different. PointNet++ and SqueezeSegV2 show an obvious downtrend, but SPG does not clearly show an accuracy drop.

For an object, the further away from the sensor, the fewer number of points it contains and the higher possibility it will be occluded. Because the features of an object with too few points are vague and confusing, even for a human, it is difficult to definitely distinguish them. Fig. 12 shows some car instances with different points in the range image view. It is difficult to recognize instances with fewer than 150 points or more than 25m. The car features become clear with the increase in points. Therefore, it is reasonable to use the point number as a measurement of instance quality.

We calculate statistics of the point number distribution of *person* and *vehicle* instances in SemanticKITTI and SemanticPOSS, as shown in Fig. 13. More than 50% of instances contain fewer than 120 points, which makes no significant contribution to model training. Although it is inevitable for 3D LiDAR datasets to contain these instances, they truly enhance the data hunger problem for data size in the 3D LiDAR semantic segmentation task.

V. EFFORTS TO SOLVE THE DATA HUNGER PROBLEM

The data hunger problem is currently a general challenge of deep learning systems [21], where large research efforts have been made for solutions in the fields of machine learning, including computer vision, intelligent vehicles, and robotics. These efforts can be broadly divided into two groups: 1) developing new methodologies that do not require a large

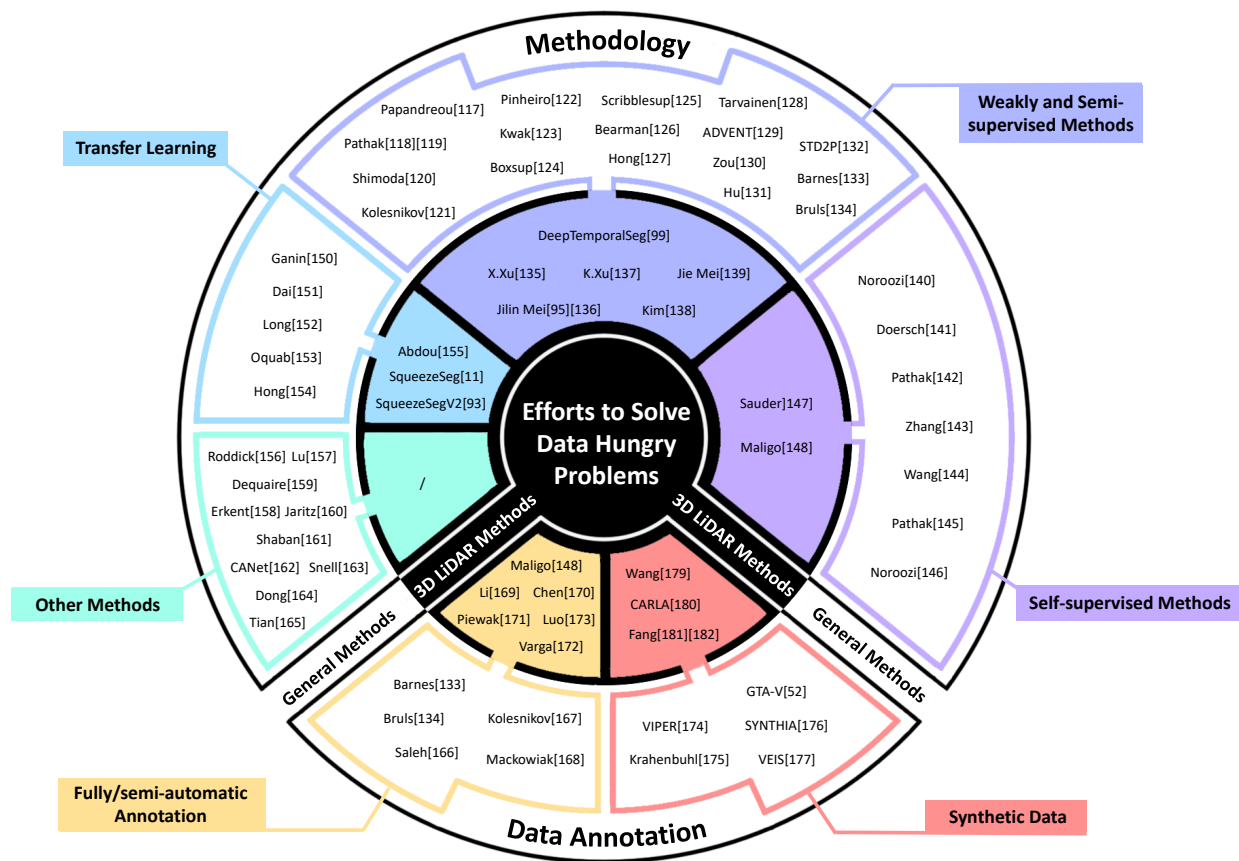


Fig. 14. Overview of efforts to solve the data hunger problem. (*General methods*: ideas come from computer vision or machine learning studies but can be heuristic or generalized to solve the data hunger problem of 3D LiDAR semantic segmentation.)

quantity of fine annotated data and 2) developing new data annotation methods that are less human intensive. Both efforts can be further divided into two groups: 1) incorporating domain knowledge for 3D LiDAR data processing and 2) general purposes that have proven to be useful on other kinds of data yet have not been adapted on 3D LiDAR applications. Hereinafter, we refer to these two groups as **3D LiDAR methods** and **general methods** for conciseness. Fig. 14 illustrates the state-of-the-art of these efforts.

A. Methodology

1) *Weakly and semi-supervised methods*: Weakly and semi-supervised methods are widely used to solve the data hunger problem with data size. They aim to mine the value of weak supervision as much as possible.

a) *General methods*: Most studies on weakly and semi-supervised semantic segmentation are investigated in the image domain. Due to the existence of large image classification datasets such as ImageNet [26], image-level annotations are easy to obtain as weak supervision of semantic segmentation [117] [118]. Sometimes, image-level weak supervision is integrated with additional information for better performance, such as prior knowledge of object size [119], saliency models indicating object regions [120] [121] and super-pixels [122] [123]. In addition to image-level labels, bounding boxes [117] [124], scribbles [125] and point supervision [126] are considered as weak supervision. Prior knowledge can provide

useful constraints of objectness [122], class-agnostic shape [127] or combinations of several priors [119]. Pseudo labeling instinctively uses model predictions to annotate unlabeled data, which is universally applicable for classification [128] and semantic segmentation [129] [130]. In addition, there are various ideas for weakly and semi-supervised learning, such as spatiotemporal constraints from videos [131], optical flow [132] or other modalities, such as GPS [133] and LiDAR [134].

b) *3D LiDAR methods*: For 3D LiDAR semantic segmentation tasks, available weak supervisions are not as abundant as image-related tasks. Xu et al. [135] used a tiny fraction of points as weak supervision. Mei et al. [136] automatically generated weak annotations based on prior human domain geometrical knowledge. Pseudo labeling was implemented by Xu et al. [137], which also introduced spatial relationships to assist the semi-supervised framework.

Additional multi-modal information is helpful for data hunger problem. Kim et al. [138] focused on a season-invariant semantic segmentation task by fusing images and 3D LiDAR information.

In addition, spatiotemporal constraints could help transit weak supervisions from adjacent points or LiDAR frames. Constraints [139] [95] can be integrated to help the model simultaneously consider intra-class compactness and inter-class separability. Dewan et al. [99] proposed a Bayes filter based method using knowledge from previous scans, which makes

the sequential predictions more temporally consistent.

2) *Self-supervised methods*: It is a common choice to pretrain a deep network with large-scale datasets such as ImageNet [26] before fine-tuning it to specific visual tasks. However, when facing the data hunger of large-scale datasets, self-supervised learning methods can play a role.

a) *General methods*: Generally, models are trained on pretext tasks to learn meaningful representations related to the target task without any human annotations. Some typical pretext tasks include context prediction [140] [141], inpainting [142], colorization [143] and temporal correlation [144] [145]. Although researchers have designed various pretext tasks, self-supervision performance is still not equal to pretraining. Several studies [146] have been made to overcome this gap.

b) *3D LiDAR methods*: Inspired by the context prediction pretext task for image semantic segmentation, Sauder et al. [147] attempted to learn from the spatial distribution by predicting randomly rearranged voxels.

In addition to learning from pretext tasks, self-supervised methods can also be implemented for clustering points with similar semantic information or common features. Maligo and Lacroix [148] classified point clouds into a large set of categories through self-supervised Gaussian mixture models and annotators can simply assign semantic labels to these categories instead of point-level annotation.

3) *Transfer learning*: The data hunger problem is not only reflected on datasets size. Diversity between different application scenarios also prevents models generalization performance. Transfer learning [149] is one approach to handle this problem.

a) *General methods*: Transfer learning methods utilize knowledge from a known source domain to new target domains. Based on the techniques, these methods can be categorized to several groups, such as adversarial-based methods [150], instances-based methods [151], mapping-based methods [152] and network-based methods [153]. It has been applied to many visual applications including semantic segmentation [154].

b) *3D LiDAR methods*: Transfer learning can help transfer knowledge from other domains to reduce the data demand of 3D LiDAR. Wu et al. [11] attempted to obtain extra training data from a LiDAR simulator GTA-V. To make the synthetic data more realistic, they transferred the noise distribution of KITTI data to synthesized data. In [93], they proposed an upgrade version for domain shift. With knowledge transferred from the real world, models trained on synthetic data can even outperform baselines trained on real datasets.

Imbalanced categories distribution is one reflection of data hunger problem. It is usually difficult to classify non-dominant categories because of their rare appearance. Abdou et al. [155] proposed a weighted self-incremental transfer learning method, which re-weighted the loss function and trained non-dominant categories preferentially.

4) *Other methods*: Semantic segmentation can be regarded as one form of scene understanding. In addition, there are many studies tackling this problem from different view. Semantic occupancy map is one of them that effectively com-

bines 3D and 2D formats, and obtains pixel-wise scene understanding from map level [156] [157]. By the way, utilizing Bayesian filter and combining temporal information [158] [159] could reduce the effect of data hunger. Multi-modality is another way that fusing 2D and 3D data for usage [158] [160] to reduce the data hunger effect. Few-shot learning aims to generalize to new tasks with only a few annotations and prior knowledge. It was introduced by Shaban et al. [161] for one-way semantic segmentation [162]. After that, N-way semantic segmentation was explored by prototype framework [163] [164] and optimization-based method [165].

B. Data Annotation

1) *Fully/semi-automatic annotation*: The high cost of pixel/point-level human annotations is one of the most important factors causing the data hunger problem. Many studies have focused on obtaining cheaper annotations by designing fully or semi-automatic annotation methods.

a) *General methods*: Fully automatic annotation often uses labels from additional sensors, such as drivable paths from GPS [133] and road marking annotations from LiDAR's intensity channel [134].

Some semi-automatic annotation methods attempt to obtain dense segmentation masks through simple clicks based on objectness priors [166] and image regions [167]. Mackowiak et al. [168] utilized the active learning idea, which makes the model select worthiest regions for hand labeling, which significantly reduces the annotation cost.

b) *3D LiDAR methods*: Fine annotations in 3D space are much more time-consuming. Methods that attempt to obtain fully automatic annotations usually depend on prior knowledge of geometry or labels from other sensors. Li et al. [169] used a decision-tree model to integrate prior knowledge among different categories and generate initialized training labels of object segments. Besides the methods based on prior knowledge, several studies [170] [171] [172] introduced labels from camera data helping 3D LiDAR annotations.

In addition, some semi-automatic methods attempted to make 3D LiDAR annotation easier and faster. Luo et al. [173] introduced an active learning framework incorporating neighbor-consistency priors to create a minimal manually annotated training set. As a result, only a few supervoxels need to be annotated. Maligo et al. [148] tried to cluster points into a large set of categories before manual annotation. Human annotators only need to group these categories and give them semantic labels through only a few shots.

2) *Synthetic data*: With the impressive progress of computer graphics, synthetic data have become an alternative to expensive and time-consuming manual annotations.

a) *General methods*: Video games are usually the first choice for synthetic data collection. Richter et al. built synthetic datasets called GTA-V [52] and VIPER [174] based on the commercial game engine Grand Theft Auto V. VIPER provides the ground truth of image semantic segmentation, instance segmentation, 3D scene layout, visual odometry and optical flow. Krahenbuhl [175] extended the data collection across three video games with more diverse scenarios.

Scenarios based on video games only provide limited freedom for customization. To overcome this drawback, SYNTHIA [176] and VEIS [177] used the Unity3D [178] development platform to design urban structures and add objects optionally.

b) 3D LiDAR methods: Several attempts have been made to obtain point-level labels of 3D LiDAR data from simulators. Wang et al. [179] proposed a pipeline for automatic generation of simulated 3D LiDAR with point-level labels. It is based on CARLA [180], a simulator for autonomous driving. There are some other general synthetic datasets, such as SYNTHIA [176] and [175], which are based on video games. They are not designed for obtaining synthetic 3D LiDAR data, but the annotations of depth images may be exploited for the acquisition of 3D LiDAR data.

Except for acquiring annotations from thorough synthetic scenes, Fang et al. [181] proposed a novel LiDAR simulator that augments real scene points with synthetic obstacles. Furthermore, real traffic flows [182] can be placed in different street view background, which is inspiring for generating synthetic data that looks real.

Synthetic data provide economical supplements for data hunger, but domain adaptation techniques are still needed when applied in the real world.

VI. FUTURE WORKS AND DISCUSSION

The "data hunger" problem is increasingly being recognized as a serious and widespread challenge for 3D LiDAR semantic segmentation. However, solutions for the problem have still been a largely underexplored domain compared with studies in computer vision and machine learning. Developing new methods that rely less on fine annotated 3D LiDAR data and developing more diversified 3D LiDAR datasets could become two main directions to focus on. Below, we elaborate on future works in these directions, followed by a discussion on the open questions, which leads to important, but until now, little studied topics.

A. Methodology

Compared to the vast number of methods using visual images, studies on 3D LiDAR data are very limited in both breadth and depth, and are usually sporadic, premature and unsystematic. Some new tendencies, such as few-shot learning, to the best of our knowledge, have not been attempted on 3D LiDAR data for semantic segmentation or relevant tasks. Below, we discuss the potential future topics on these aspects.

1) Bounding boxes: The bounding box has been used as a weak supervision signal in developing many semantic segmentation methods of visual images [124] [117], and bounding boxes are actually available in many open datasets [36] [45] [46] [49], as reviewed in Table I. Can we make use of this information in processing 3D LiDAR data? The idea of solving the data hunger problem in 3D LiDAR seems to be absent in the efforts until now.

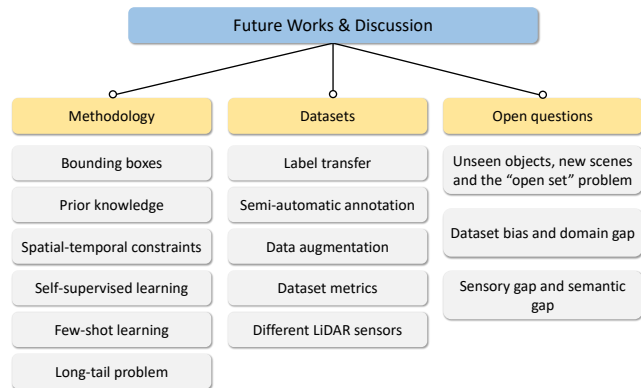


Fig. 15. Overview of future works and open questions.

2) Prior knowledge: Different from visual images, 3D LiDAR captures real-world data of true physical size and spatial geometry. Many prior knowledge can be used. For example, an approximate elevation of the ground surface and rough size of objects. These prior knowledge can greatly help to save learning costs.

3) Spatial-temporal constraints: Semantic segmentation of video has been studied in computer vision and multimedia societies [183]; however, 3D LiDAR data have been mostly processed frame by frame, which ignores temporal continuity and coherence cues. It can help to save computation time, improve accuracy and reduce the needs of fine annotated data.

4) Self-supervised learning: To make use of the large quantity of unlabeled data, self-supervised learning utilizes pretext tasks. Such an idea is still rare in 3D LiDAR processing, whereas various pretext tasks have been designed on images to learn meaningful representations. It may inspire new directions in the 3D LiDAR domain.

5) Few-shot learning: Few-shot learning generalizes new tasks from a few supervisions and prior knowledge, as a human being does. It has even moved forward to zero-shot semantic segmentation [184], which transfers semantic similarities from linguistic features. The idea of few-shot learning is inspiring, but the studies are still in the early stages and has not been applied to 3D LiDAR data.

6) The long-tail problem: 3D LiDAR datasets are long-tailed. As discussed in Section II, *road*, *building* and *vegetation* occupy large proportions, whereas *people*, *car* and *riders* are rare and thus difficult to model. Testing on such datasets reveals the performance of the major categories, while those of the minor ones are often overlooked. Long-tail has been a general problem in machine learning that has been studied extensively [185]. The problem is even severe of 3D LiDAR datasets due to the way of data acquisition and object occupation at natural scenes, whereas it has been few addressed in 3D semantic segmentation studies.

B. Datasets

The superior performance of deep learning methods is usually established on a large quantity of fine annotated datasets. However, currently, 3D LiDAR datasets are very limited in

terms of both size and diversity. How can data generation be more efficient and less labor intensive? More research is needed, where some potential topics are discussed below.

1) *Label transfer*: Label transfer is a cheap solution to obtain more 3D LiDAR annotations, which borrows labels from other modalities, such as images [171] [172] [170]. However, existing methods usually project image results to 3D LiDAR data, where both correct and incorrect annotations are transferred. Error detection mechanisms are needed in this procedure, where prior knowledge, such as the size, geometry, spatial and temporal coherence of 3D LiDAR data, could be important cues to filter false alarms.

2) *Semi-automatic annotation*: Semiautomatic annotation is an attempt to find a balance between the efficiency and quality of data generation. Some studies [186] use semi-automatic methods to accelerate the labeling of 3D bounding boxes. Semi-automatic annotation for point-level semantic segmentation is more complicated. Some CRF-based methods [187] are developed, but the cost improvements are still limited. In the future, techniques such as active learning [188] and online learning may further boost the semi-automatic annotation process.

3) *Data augmentation*: Data augmentation is a commonly used trick for enriching data diversity, which has been proven to achieve gains compared to architectural improvements, both in 2D image [189] and 3D LiDAR object detection tasks [190]. However, common augmentation operations such as random flip, rotation and scaling, which are useful for single objects, may cause discordance of context elements for semantic segmentation. To the best of our knowledge, there is no systematic research on point-wise data augmentation for 3D LiDAR semantic segmentation, so there is considerable room for growth.

4) *Dataset metrics*: It is needed to guide dataset generation, e.g. building datasets of new scenes but avoiding generating similar scenes repetition. It is needed too to guide dataset-based testing more efficiently. A dataset is composed of very limited snapshots of real-world scenes. It is very important for real-world applications such as autonomous driving to have the knowledge what performance could be achieved at a target scene, what difference of scenes can the model adapt to, and what dataset could lead a test result that reflects objectively the performance at real world. Many metrics have been developed to evaluate model performance, while we have found no widely accepted metric of dataset that is able to answer the above needs.

5) *Different LiDAR sensors*: In recent years, many LiDAR sensors have been developed of different specifications by different manufacturers, and according to system configurations, 3D points are measured from viewpoints at different elevations and angles, which could vary object appearance and category distribution of the datasets largely. As listed in Table I, most datasets are developed by a particular LiDAR sensor of a particular system configuration. The challenges from different sensors are not fully recognized now, which makes it hard to train a 3D semantic segmentation model on more datasets, and hard to transfer a model to the ones with other types of sensor

input. These problems need to be addressed in future from both dataset and methodological aspects.

C. Open Questions

1) *Unseen objects, new scenes, and the "open set" problem*: Currently, studies mostly design algorithms and evaluate model performance in a "closed set" [191], which assumes that the testing set obeys the same distribution as the training one. However, real world applications are an "open set" problem, which requires deep models to deal with unseen objects and new scenes. It has been a general problem of deep models, which will always be data hungry in unseen categories and new scenarios. However, the problem is even severe for the applications like autonomous driving, where some categories are unseen or rare in datasets but need to be handled in real applications. Therefore data hunger may always exist, it is far more important of the model to be aware of when it is unsure.

2) *Dataset bias and domain gap*: It is inevitable for actual datasets to be a biased sampling of the real world. Dataset bias is a general problem of machine learning. Many studies have been addressed to explore the bias [21] by cross-dataset experiments, undo the damage [192] by modeling bias vector, and [193] found that many existing ad hoc learning algorithms for undoing the dataset bias do not help for CNN features. The most concerned dataset bias in 3D semantic segmentation task is domain gap, which exhibits in both model and dataset aspects. The former is usually solved by transfer learning [] to adapt a model from one domain to another. However, domain gap among datasets is less explored. As discussed in Section IV, mixing multiple data sets in training may not improve model accuracy, and testing model on a dataset with a large domain gap may also cause a significant performance degradation, limiting the usefulness of the test results. Making use of different dataset needs rigorous study, where dataset metrics to evaluate domain gap quantitatively may be one of the keys.

3) *Sensory gap and semantic gap*: Sensory gap exists between objects in the real world and in data due to sensory limitation, e.g. partial observation, occlusion and sparse point sampling. Semantic gap means people understand an object based on the knowledge that may beyond those provided by the data, whereas a machine does not. For example, a tree could be measured on its straight trunk, which looks very similar to a pole from the data appearance at the moment. In addition, there are many types of bicycles and motorcycles, from small to large scales, where sensory data may not be distinguishable on functional categorization, and an object of the same functional category may have largely different appearance, and in different countries/regions. These sensory and semantic gaps bring great difficulties in developing a general category list for dataset sharing, which needs scientific studies at the communities' level.

VII. CONCLUSION

In this research, a comprehensive survey and experimental study is conducted to seek answers to the question: 'Are we

hungry for 3D LiDAR data for semantic segmentation?’ The following studies are addressed. First, a broad review to the main 3D LiDAR datasets is conducted, followed by a statistical analysis on three representative datasets to gain an in-depth view on the datasets’ size and diversity, which are the critical factors in learning deep models. Second, a systematic review to the state-of-the-art 3D semantic segmentation is conducted, followed by experiments and cross examinations of three representative deep learning methods to find out how the size and diversity of the datasets affect deep models’ performance. The major findings in the above studies are:

- 1) Due to the uneven spatial distribution of 3D LiDAR data, large amount of points could be scanned on the same objects that bring few novel information, and large portion of data points belong to the category of the objects nearby sensor’s viewpoint, e.g. *road*, the datasets are therefore extremely long-tailed.
- 2) Scenes could be very diverse that are not directly correlated with geographic location. The existing 3D LiDAR datasets reflect only a very small set of real world scenes, whereas they exhibit insufficient inner-dataset diversity, while large cross-dataset difference.
- 3) Due to the large domain gap, mixing multiple datasets in training may not improve model accuracy, and testing model on a dataset with a large domain gap may also cause a significant performance degradation, limiting the usefulness of the test results.

Finally, a systematic survey to the existing efforts to solve the data hunger problem is conducted on both methodological and dataset’s viewpoints, followed by an insightful discussion of remaining problems and open questions leading to potential topics in future works.

Towards the robotic and autonomous driving applications at complex real-worlds, data hunger may always exist. On one hand, it is important to develop methods rely on less fine annotated data for training, and facing rare/unseen objects, it is far more important of the model to be aware when it’s unsure. On the other hand, metrics are needed to measure the domain gap of datasets/scenes, which is needed to guide dataset generation and model testing more efficiently. A general definition of category list is also needed for dataset sharing, which requires scientific study through international collaboration.

REFERENCES

- [1] S. Thrun, M. Montemerlo, H. Dahlkamp, D. Stavens, A. Aron, J. Diebel, P. Fong, J. Gale, M. Halpenny, G. Hoffmann *et al.*, “Stanley: The robot that won the DARPA grand challenge,” *Journal of Field Robotics*, vol. 23, no. 9, pp. 661–692, 2006.
- [2] B. J. Patz, Y. Papelis, R. Pillat, G. Stein, and D. Harper, “A practical approach to robotic design for the DARPA urban challenge,” *Journal of Field Robotics*, vol. 25, no. 8, pp. 528–566, 2008.
- [3] J. Zhang and S. Singh, “LOAM: LiDAR odometry and mapping in real-time,” in *Robotics: Science and Systems*, vol. 2, no. 9, 2014.
- [4] W. Hess, D. Kohler, H. Rapp, and D. Andor, “Real-time loop closure in 2D LiDAR slam,” in *2016 IEEE International Conference on Robotics and Automation*. IEEE, 2016, pp. 1271–1278.
- [5] B. Li, T. Zhang, and T. Xia, “Vehicle detection from 3D LiDAR using fully convolutional network,” *arXiv preprint arXiv:1608.07916*, 2016.
- [6] X. Chen, H. Ma, J. Wan, B. Li, and T. Xia, “Multi-view 3D object detection network for autonomous driving,” in *IEEE Conference on Computer Vision and Pattern Recognition*, 2017, pp. 1907–1915.
- [7] T. Hackel, N. Savinov, L. Ladicky, J. D. Wegner, K. Schindler, and M. Pollefeys, “Semantic3D.net: A new large-scale point cloud classification benchmark,” *arXiv preprint arXiv:1704.03847*, 2017.
- [8] J. Behley, M. Garbade, A. Milioto, J. Quenzel, S. Behnke, C. Stachniss, and J. Gall, “SemanticKITTI: A dataset for semantic scene understanding of LiDAR sequences,” in *IEEE International Conference on Computer Vision*, 2019, pp. 9297–9307.
- [9] R. B. Rusu and S. Cousins, “3D is here: Point cloud library (pcl),” in *2011 IEEE International Conference on Robotics and Automation*. IEEE, 2011, pp. 1–4.
- [10] C. R. Qi, H. Su, K. Mo, and L. J. Guibas, “PointNet: Deep learning on point sets for 3D classification and segmentation,” in *IEEE Conference on Computer Vision and Pattern Recognition*, 2017, pp. 652–660.
- [11] B. Wu, A. Wan, X. Yue, and K. Keutzer, “SqueezeSeg: Convolutional neural nets with recurrent CRF for real-time road-object segmentation from 3D LiDAR point cloud,” in *IEEE International Conference on Robotics and Automation*. IEEE, 2018, pp. 1887–1893.
- [12] A. Garcia-Garcia, S. Orts-Escobedo, S. Oprea, V. Villena-Martinez, and J. Garcia-Rodriguez, “A review on deep learning techniques applied to semantic segmentation,” *arXiv preprint arXiv:1704.06857*, 2017.
- [13] H. Yu, Z. Yang, L. Tan, Y. Wang, W. Sun, M. Sun, and Y. Tang, “Methods and datasets on semantic segmentation: A review,” *Neurocomputing*, vol. 304, pp. 82–103, 2018.
- [14] Y. Xie, J. Tian, and X. X. Zhu, “A review of point cloud semantic segmentation,” *arXiv preprint arXiv:1908.08854*, 2019.
- [15] Y. Guo, H. Wang, Q. Hu, H. Liu, L. Liu, and M. Bennamoun, “Deep learning for 3D point clouds: A survey,” *arXiv preprint arXiv:1912.12033*, 2019.
- [16] H. Zhu, F. Meng, J. Cai, and S. Lu, “Beyond pixels: A comprehensive survey from bottom-up to semantic image segmentation and cosegmentation,” *Journal of Visual Communication and Image Representation*, vol. 34, pp. 12–27, 2016.
- [17] Y. LeCun, Y. Bengio, and G. Hinton, “Deep learning,” *Nature*, vol. 521, no. 7553, pp. 436–444, 2015.
- [18] J. Schmidhuber, “Deep learning in neural networks: An overview,” *Neural Networks*, vol. 61, pp. 85–117, 2015.
- [19] J. Long, E. Shelhamer, and T. Darrell, “Fully convolutional networks for semantic segmentation,” in *IEEE Conference on Computer Vision and Pattern Recognition*, 2015, pp. 3431–3440.
- [20] X.-W. Chen and X. Lin, “Big data deep learning: challenges and perspectives,” *IEEE access*, vol. 2, pp. 514–525, 2014.
- [21] A. Torralba and A. A. Efros, “Unbiased look at dataset bias,” in *IEEE Conference on Computer Vision and Pattern Recognition*. IEEE, 2011, pp. 1521–1528.
- [22] C. Sun, A. Shrivastava, S. Singh, and A. Gupta, “Revisiting unreasonable effectiveness of data in deep learning era,” in *IEEE International Conference on Computer Vision*, 2017, pp. 843–852.
- [23] G. Marcus, “Deep learning: A critical appraisal,” *arXiv preprint arXiv:1801.00631*, 2018.
- [24] I. Armeni, O. Sener, A. R. Zamir, H. Jiang, I. Brilakis, M. Fischer, and S. Savarese, “3D semantic parsing of large-scale indoor spaces,” in *IEEE Conference on Computer Vision and Pattern Recognition*, 2016, pp. 1534–1543.
- [25] M. Everingham, S. A. Eslami, L. Van Gool, C. K. Williams, J. Winn, and A. Zisserman, “The PASCAL visual object classes challenge: A retrospective,” *International Journal of Computer Vision*, vol. 111, no. 1, pp. 98–136, 2015.
- [26] J. Deng, W. Dong, R. Socher, L.-J. Li, K. Li, and L. Fei-Fei, “ImageNet: A large-scale hierarchical image database,” in *IEEE Conference on Computer Vision and Pattern Recognition*. IEEE, 2009, pp. 248–255.
- [27] A. Nguyen and B. Le, “3D point cloud segmentation: A survey,” in *IEEE Conference on Robotics, Automation and Mechatronics*. IEEE, 2013, pp. 225–230.
- [28] E. Grilli, F. Menna, and F. Remondino, “A review of point clouds segmentation and classification algorithms,” *The International Archives of Photogrammetry, Remote Sensing and Spatial Information Sciences*, vol. 42, p. 339, 2017.
- [29] F. Lateef and Y. Ruichek, “Survey on semantic segmentation using deep learning techniques,” *Neurocomputing*, vol. 338, pp. 321–348, 2019.
- [30] K. Vodrahalli and A. K. Bhowmik, “3D computer vision based on machine learning with deep neural networks: A review,” *Journal of the Society for Information Display*, vol. 25, no. 11, pp. 676–694, 2017.
- [31] A. Ioannidou, E. Chatzilari, S. Nikolopoulos, and I. Kompatsiaris, “Deep learning advances in computer vision with 3D data: A survey,” *ACM Computing Surveys (CSUR)*, vol. 50, no. 2, pp. 1–38, 2017.

- [32] D. Griffiths and J. Boehm, "A review on deep learning techniques for 3D sensed data classification," *Remote Sensing*, vol. 11, no. 12, p. 1499, 2019.
- [33] S. A. Bello, S. Yu, and C. Wang, "Review: deep learning on 3D point clouds," *arXiv preprint arXiv:2001.06280*, 2020.
- [34] D. Feng, C. Haase-Schütz, L. Rosenbaum, H. Hertlein, C. Glaeser, F. Timm, W. Wiesbeck, and K. Dietmayer, "Deep multi-modal object detection and semantic segmentation for autonomous driving: Datasets, methods, and challenges," *IEEE Transactions on Intelligent Transportation Systems*, 2020.
- [35] X. Roynard, J.-E. Deschaud, and F. Goulette, "Paris-Lille-3D: A large and high-quality ground-truth urban point cloud dataset for automatic segmentation and classification," *The International Journal of Robotics Research*, vol. 37, no. 6, pp. 545–557, 2018.
- [36] A. Geiger, P. Lenz, and R. Urtasun, "Are we ready for autonomous driving? the KITTI vision benchmark suite," in *IEEE Conference on Computer Vision and Pattern Recognition*. IEEE, 2012, pp. 3354–3361.
- [37] D. Griffiths and J. Boehm, "Synthcity: A large scale synthetic point cloud," *arXiv preprint arXiv:1907.04758*, 2019.
- [38] D. Munoz, J. A. Bagnell, N. Vandapel, and M. Hebert, "Contextual classification with functional max-margin markov networks," in *IEEE Conference on Computer Vision and Pattern Recognition*. IEEE, 2009, pp. 975–982.
- [39] A. Serna, B. Marcotegui, F. Goulette, and J.-E. Deschaud, "Paris-rue-madame database," in *International Conference on Pattern Recognition Applications and Methods*, ser. ICPRAM 2014. Setubal, PRT: SCITEPRESS - Science and Technology Publications, Lda, 2014, p. 819–824.
- [40] B. Vallet, M. Brédif, A. Serna, B. Marcotegui, and N. Paparoditis, "Ter-mobilita/iqmulus urban point cloud analysis benchmark," *Computers & Graphics*, vol. 49, pp. 126–133, 2015.
- [41] J. Gehrung, M. Hebel, M. Arens, and U. Stilla, "An approach to extract moving objects from mls data using a volumetric background representation," *ISPRS Annals of the Photogrammetry, Remote Sensing and Spatial Information Sciences*, vol. 4, p. 107, 2017.
- [42] M. De Deuge, A. Quadros, C. Hung, and B. Douillard, "Unsupervised feature learning for classification of outdoor 3D scans," in *Australasian Conference on Robotics and Automation*, vol. 2, 2013, p. 1.
- [43] Y. Pan, B. Gao, J. Mei, S. Geng, C. Li, and H. Zhao, "SemanticPOSS: A point cloud dataset with large quantity of dynamic instances," *arXiv preprint arXiv:2002.09147*, 2020.
- [44] J. Geyer, Y. Kassahun, M. Mahmudi, X. Ricou, R. Durgesh, A. S. Chung, L. Hauswald, V. H. Pham, M. Mühlegg, S. Dorn *et al.*, "A2Ds2: Audi autonomous driving dataset," *arXiv preprint arXiv:2004.06320*, 2020.
- [45] A. Patil, S. Malla, H. Gang, and Y.-T. Chen, "The H3D dataset for full-surround 3D multi-object detection and tracking in crowded urban scenes," in *International Conference on Robotics and Automation*. IEEE, 2019, pp. 9552–9557.
- [46] H. Caesar, V. Bankiti, A. H. Lang, S. Vora, V. E. Liong, Q. Xu, A. Krishnan, Y. Pan, G. Baldan, and O. Beijbom, "nuScenes: A multimodal dataset for autonomous driving," *arXiv preprint arXiv:1903.11027*, 2019.
- [47] R. Kesten, M. Usman, J. Houston, T. Pandya, K. Nadhamuni, A. Ferreira, M. Yuan, B. Low, A. Jain, P. Ondruska, S. Omari, S. Shah, A. Kulkarni, A. Kazakova, C. Tao, L. Platinsky, W. Jiang, and V. Shet, "Lyft level 5 perception dataset 2020," <https://level5.lyft.com/dataset/>, 2019.
- [48] M.-F. Chang, J. Lambert, P. Sangkloy, J. Singh, S. Bak, A. Hartnett, D. Wang, P. Carr, S. Lucey, D. Ramanan *et al.*, "Argoverse: 3D tracking and forecasting with rich maps," in *IEEE Conference on Computer Vision and Pattern Recognition*, 2019, pp. 8748–8757.
- [49] P. Sun, H. Kretschmar, X. Dotiwalla, A. Chouard, V. Patnaik, P. Tsui, J. Guo, Y. Zhou, Y. Chai, B. Caine *et al.*, "Scalability in perception for autonomous driving: Waymo open dataset," *arXiv*, pp. arXiv–1912, 2019.
- [50] Q.-H. Pham, P. Sevestre, R. S. Pahwa, H. Zhan, C. H. Pang, Y. Chen, A. Mustafa, V. Chandrasekhar, and J. Lin, "A*3D dataset: Towards autonomous driving in challenging environments," in *IEEE International Conference on Robotics and Automation*. IEEE, 2020, pp. 2267–2273.
- [51] M. Bijelic, T. Gruber, F. Mannan, F. Kraus, W. Ritter, K. Dietmayer, and F. Heide, "Seeing through fog without seeing fog: Deep multimodal sensor fusion in unseen adverse weather," in *IEEE Conference on Computer Vision and Pattern Recognition*, 2020, pp. 11 682–11 692.
- [52] S. R. Richter, V. Vineet, S. Roth, and V. Koltun, "Playing for data: Ground truth from computer games," in *European Conference on Computer Vision*. Springer, 2016, pp. 102–118.
- [53] M. Cordts, M. Omran, S. Ramos, T. Rehfeld, M. Enzweiler, R. Benenson, U. Franke, S. Roth, and B. Schiele, "The Cityscapes dataset for semantic urban scene understanding," in *IEEE Conference on Computer Vision and Pattern Recognition*, 2016, pp. 3213–3223.
- [54] N. Silberman, D. Hoiem, P. Kohli, and R. Fergus, "Indoor segmentation and support inference from RGBD images," in *European Conference on Computer Vision*. Springer, 2012, pp. 746–760.
- [55] A. Dai, A. X. Chang, M. Savva, M. Halber, T. Funkhouser, and M. Nießner, "ScanNet: Richly-annotated 3D reconstructions of indoor scenes," in *IEEE Conference on Computer Vision and Pattern Recognition*, 2017, pp. 5828–5839.
- [56] X. Huang, P. Wang, X. Cheng, D. Zhou, Q. Geng, and R. Yang, "The ApolloScape open dataset for autonomous driving and its application," *arXiv preprint arXiv:1803.06184*, 2018.
- [57] Q. Hu, B. Yang, L. Xie, S. Rosa, Y. Guo, Z. Wang, N. Trigoni, and A. Markham, "RandLA-Net: Efficient semantic segmentation of large-scale point clouds," *arXiv preprint arXiv:1911.11236*, 2019.
- [58] A. Kirillov, K. He, R. Girshick, C. Rother, and P. Dollár, "Panoptic segmentation," in *IEEE Conference on Computer Vision and Pattern Recognition*, 2019, pp. 9404–9413.
- [59] Hesaitech.com, "Pandora-HESAI," <https://www.hesaitech.com/en/Pandora>.
- [60] A. Anand, H. S. Koppula, T. Joachims, and A. Saxena, "Contextually guided semantic labeling and search for three-dimensional point clouds," *The International Journal of Robotics Research*, vol. 32, no. 1, pp. 19–34, 2013.
- [61] D. Wolf, J. Prankl, and M. Vincze, "Fast semantic segmentation of 3D point clouds using a dense CRF with learned parameters," in *IEEE International Conference on Robotics and Automation*. IEEE, 2015, pp. 4867–4873.
- [62] A. Golovinskiy, V. G. Kim, and T. Funkhouser, "Shape-based recognition of 3d point clouds in urban environments," in *IEEE International Conference on Computer Vision*. IEEE, 2009, pp. 2154–2161.
- [63] T. Hackel, J. D. Wegner, and K. Schindler, "Fast semantic segmentation of 3d point clouds with strongly varying density," *ISPRS annals of the photogrammetry, remote sensing and spatial information sciences*, vol. 3, pp. 177–184, 2016.
- [64] M. Weinmann, B. Jutzi, S. Hinz, and C. Mallet, "Semantic point cloud interpretation based on optimal neighborhoods, relevant features and efficient classifiers," *ISPRS Journal of Photogrammetry and Remote Sensing*, vol. 105, pp. 286–304, 2015.
- [65] D. Anguelov, B. Taskarf, V. Chatalbashev, D. Koller, D. Gupta, G. Heitz, and A. Ng, "Discriminative learning of markov random fields for segmentation of 3D scan data," in *IEEE Conference on Computer Vision and Pattern Recognition*, vol. 2. IEEE, 2005, pp. 169–176.
- [66] R. Triebel, K. Kersting, and W. Burgard, "Robust 3D scan point classification using associative markov networks," in *IEEE International Conference on Robotics and Automation*. IEEE, 2006, pp. 2603–2608.
- [67] C. R. Qi, L. Yi, H. Su, and L. J. Guibas, "PointNet++: Deep hierarchical feature learning on point sets in a metric space," in *Advances in Neural Information Processing Systems*, 2017, pp. 5099–5108.
- [68] F. Engelmann, T. Kontogianni, A. Hermans, and B. Leibe, "Exploring spatial context for 3D semantic segmentation of point clouds," in *IEEE International Conference on Computer Vision Workshops*, 2017, pp. 716–724.
- [69] M. Jiang, Y. Wu, T. Zhao, Z. Zhao, and C. Lu, "PointSIFT: A SIFT-like network module for 3D point cloud semantic segmentation," *arXiv preprint arXiv:1807.00652*, 2018.
- [70] F. Engelmann, T. Kontogianni, J. Schult, and B. Leibe, "Know what your neighbors do: 3D semantic segmentation of point clouds," in *European Conference on Computer Vision*, 2018, pp. 0–0.
- [71] J. Li, B. M. Chen, and G. Hee Lee, "SO-Net: Self-organizing network for point cloud analysis," in *IEEE Conference on Computer Vision and Pattern Recognition*, 2018, pp. 9397–9406.
- [72] J. Yang, Q. Zhang, B. Ni, L. Li, J. Liu, M. Zhou, and Q. Tian, "Modeling point clouds with self-attention and gumbel subset sampling," in *IEEE Conference on Computer Vision and Pattern Recognition*, 2019, pp. 3323–3332.
- [73] L.-Z. Chen, X.-Y. Li, D.-P. Fan, M.-M. Cheng, K. Wang, and S.-P. Lu, "LSANet: Feature learning on point sets by local spatial attention," *arXiv preprint arXiv:1905.05442*, 2019.
- [74] K. Zhiheng and L. Ning, "PyramNet: Point cloud pyramid attention network and graph embedding module for classification and segmentation," *arXiv preprint arXiv:1906.03299*, 2019.

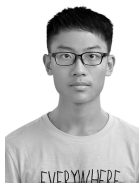
- [75] Y. Li, R. Bu, M. Sun, W. Wu, X. Di, and B. Chen, "PointCNN: Convolution on x-transformed points," in *Advances in neural information processing systems*, 2018, pp. 820–830.
- [76] A. Komarichev, Z. Zhong, and J. Hua, "A-CNN: Annularly convolutional neural networks on point clouds," in *IEEE Conference on Computer Vision and Pattern Recognition*, 2019, pp. 7421–7430.
- [77] H. Thomas, C. R. Qi, J.-E. Deschaut, B. Marcotegui, F. Goulette, and L. J. Guibas, "KPConv: Flexible and deformable convolution for point clouds," in *IEEE International Conference on Computer Vision*, 2019, pp. 6411–6420.
- [78] F. Engelmann, T. Kontogianni, and B. Leibe, "Dilated point convolutions: On the receptive field of point convolutions," *arXiv preprint arXiv:1907.12046*, 2019.
- [79] L. Pan, P. Wang, and C.-M. Chew, "PointAtrousNet: Point atrous convolution for point cloud analysis," *IEEE Robotics and Automation Letters*, vol. 4, no. 4, pp. 4035–4041, 2019.
- [80] L. Pan, C.-M. Chew, and G. H. Lee, "PointAtrousGraph: Deep hierarchical encoder-decoder with atrous convolution for point clouds," *arXiv preprint arXiv:1907.09798*, 2019.
- [81] M. Tatarchenko, J. Park, V. Koltun, and Q.-Y. Zhou, "Tangent convolutions for dense prediction in 3D," in *IEEE Conference on Computer Vision and Pattern Recognition*, 2018, pp. 3887–3896.
- [82] Z. Zhao, M. Liu, and K. Ramani, "DAR-Net: Dynamic aggregation network for semantic scene segmentation," *arXiv preprint arXiv:1907.12022*, 2019.
- [83] Z. Zhang, B.-S. Hua, and S.-K. Yeung, "ShellNet: Efficient point cloud convolutional neural networks using concentric shells statistics," in *IEEE International Conference on Computer Vision*, 2019, pp. 1607–1616.
- [84] Z. Liu, H. Tang, Y. Lin, and S. Han, "Point-voxel cnn for efficient 3D deep learning," in *Advances in Neural Information Processing Systems*, 2019, pp. 965–975.
- [85] Q. Huang, W. Wang, and U. Neumann, "Recurrent slice networks for 3D segmentation of point clouds," in *IEEE Conference on Computer Vision and Pattern Recognition*, 2018, pp. 2626–2635.
- [86] H. Su, V. Jampani, D. Sun, S. Maji, E. Kalogerakis, M.-H. Yang, and J. Kautz, "SplatNet: Sparse lattice networks for point cloud processing," in *IEEE Conference on Computer Vision and Pattern Recognition*, 2018, pp. 2530–2539.
- [87] V. Jampani, M. Kiefel, and P. V. Gehler, "Learning sparse high dimensional filters: Image filtering, dense CRFs and bilateral neural networks," in *IEEE Conference on Computer Vision and Pattern Recognition*, 2016, pp. 4452–4461.
- [88] R. A. Rosu, P. Schütt, J. Quenzel, and S. Behnke, "LatticeNet: Fast point cloud segmentation using permutohedral lattices," *arXiv preprint arXiv:1912.05905*, 2019.
- [89] O. Ronneberger, P. Fischer, and T. Brox, "U-Net: Convolutional networks for biomedical image segmentation," in *International Conference on Medical Image Computing and Computer-Assisted Intervention*. Springer, 2015, pp. 234–241.
- [90] F. J. Lawin, M. Danelljan, P. Tosteberg, G. Bhat, F. S. Khan, and M. Felsberg, "Deep projective 3D semantic segmentation," in *International Conference on Computer Analysis of Images and Patterns*. Springer, 2017, pp. 95–107.
- [91] A. Boulch, B. L. Saux, and N. Audebert, "Unstructured point cloud semantic labeling using deep segmentation networks," in *Workshop on 3D Object Retrieval*, ser. 3DOR '17. Goslar, DEU: Eurographics Association, 2017, p. 17–24.
- [92] F. N. Iandola, S. Han, M. W. Moskewicz, K. Ashraf, W. J. Dally, and K. Keutzer, "SqueezeNet: AlexNet-level accuracy with 50x fewer parameters and < 0.5MB model size," *arXiv preprint arXiv:1602.07360*, 2016.
- [93] B. Wu, X. Zhou, S. Zhao, X. Yue, and K. Keutzer, "SqueezeSegV2: Improved model structure and unsupervised domain adaptation for road-object segmentation from a LiDAR point cloud," in *International Conference on Robotics and Automation*. IEEE, 2019, pp. 4376–4382.
- [94] C. Xu, B. Wu, Z. Wang, W. Zhan, P. Vajda, K. Keutzer, and M. Tomizuka, "SqueezeSegV3: Spatially-adaptive convolution for efficient point-cloud segmentation," *arXiv preprint arXiv:2004.01803*, 2020.
- [95] J. Mei, B. Gao, D. Xu, W. Yao, X. Zhao, and H. Zhao, "Semantic segmentation of 3D LiDAR data in dynamic scene using semi-supervised learning," *IEEE Transactions on Intelligent Transportation Systems*, 2019.
- [96] A. Milioto, I. Vizzo, J. Behley, and C. Stachniss, "RangeNet++: Fast and accurate LiDAR semantic segmentation," in *IEEE/RSJ International Conference on Intelligent Robots and Systems*, 2019.
- [97] P. Biasutti, V. Lepetit, J.-F. Aujol, M. Brédif, and A. Bugeau, "LU-Net: An efficient network for 3D LiDAR point cloud semantic segmentation based on end-to-end-learned 3D features and U-Net," in *IEEE International Conference on Computer Vision Workshops*, 2019, pp. 0–0.
- [98] I. Alonso, L. Riazuelo, L. Montesano, and A. C. Murillo, "3D-MiniNet: Learning a 2D representation from point clouds for fast and efficient 3D LiDAR semantic segmentation," *arXiv preprint arXiv:2002.10893*, 2020.
- [99] A. Dewan and W. Burgard, "DeepTemporalSeg: Temporally consistent semantic segmentation of 3D LiDAR scans," *arXiv preprint arXiv:1906.06962*, 2019.
- [100] W. Zhang, C. Zhou, J. Yang, and K. Huang, "LiSeg: Lightweight road-object semantic segmentation in 3D LiDAR scans for autonomous driving," in *IEEE Intelligent Vehicles Symposium*. IEEE, 2018, pp. 1021–1026.
- [101] Y. Wang, T. Shi, P. Yun, L. Tai, and M. Liu, "PointSeg: Real-time semantic segmentation based on 3D LiDAR point cloud," *arXiv preprint arXiv:1807.06288*, 2018.
- [102] P. Biasutti, A. Bugeau, J.-F. Aujol, and M. Brédif, "RIU-Net: Embarassingly simple semantic segmentation of 3D LiDAR point cloud," *arXiv preprint arXiv:1905.08748*, 2019.
- [103] E. E. Aksoy, S. Baci, and S. Cavdar, "SalsaNet: Fast road and vehicle segmentation in LiDAR point clouds for autonomous driving," *arXiv preprint arXiv:1909.08291*, 2019.
- [104] T. Cortinhal, G. Tzelepis, and E. E. Aksoy, "SalsaNext: Fast, uncertainty-aware semantic segmentation of LiDAR point clouds for autonomous driving," *arXiv preprint arXiv:2003.03653*, 2020.
- [105] J. Huang and S. You, "Point cloud labeling using 3D convolutional neural network," in *International Conference on Pattern Recognition*. IEEE, 2016, pp. 2670–2675.
- [106] L. Tchapmi, C. Choy, I. Armeni, J. Gwak, and S. Savarese, "Segcloud: Semantic segmentation of 3D point clouds," in *2017 international conference on 3D vision*. IEEE, 2017, pp. 537–547.
- [107] D. Rethage, J. Wald, J. Sturm, N. Navab, and F. Tombari, "Fully-convolutional point networks for large-scale point clouds," in *European Conference on Computer Vision*, 2018, pp. 596–611.
- [108] F. Liu, S. Li, L. Zhang, C. Zhou, R. Ye, Y. Wang, and J. Lu, "3DCNN-DQN-RNN: A deep reinforcement learning framework for semantic parsing of large-scale 3D point clouds," in *IEEE International Conference on Computer Vision*, 2017, pp. 5678–5687.
- [109] B. Graham, M. Engelcke, and L. van der Maaten, "3D semantic segmentation with submanifold sparse convolutional networks," in *IEEE Conference on Computer Vision and Pattern Recognition*, 2018, pp. 9224–9232.
- [110] C. Zhang, W. Luo, and R. Urtasun, "Efficient convolutions for real-time semantic segmentation of 3D point clouds," in *International Conference on 3D Vision*. IEEE, 2018, pp. 399–408.
- [111] H.-Y. Meng, L. Gao, Y.-K. Lai, and D. Manocha, "VV-Net: Voxel vae net with group convolutions for point cloud segmentation," in *IEEE International Conference on Computer Vision*, 2019, pp. 8500–8508.
- [112] H. Radi and W. Ali, "VolMap: A real-time model for semantic segmentation of a LiDAR surrounding view," *arXiv preprint arXiv:1906.11873*, 2019.
- [113] L. Landrieu and M. Simonovsky, "Large-scale point cloud semantic segmentation with superpoint graphs," in *IEEE Conference on Computer Vision and Pattern Recognition*, 2018, pp. 4558–4567.
- [114] L. Wang, Y. Huang, Y. Hou, S. Zhang, and J. Shan, "Graph attention convolution for point cloud semantic segmentation," in *IEEE Conference on Computer Vision and Pattern Recognition*, 2019, pp. 10296–10305.
- [115] L. Jiang, H. Zhao, S. Liu, X. Shen, C.-W. Fu, and J. Jia, "Hierarchical point-edge interaction network for point cloud semantic segmentation," in *IEEE International Conference on Computer Vision*, 2019, pp. 10433–10441.
- [116] Y. Wang, Y. Sun, Z. Liu, S. E. Sarma, M. M. Bronstein, and J. M. Solomon, "Dynamic graph CNN for learning on point clouds," *ACM Transactions On Graphics (tog)*, vol. 38, no. 5, pp. 1–12, 2019.
- [117] G. Papandreou, L.-C. Chen, K. P. Murphy, and A. L. Yuille, "Weakly- and semi-supervised learning of a deep convolutional network for semantic image segmentation," in *IEEE International Conference on Computer Vision*, 2015, pp. 1742–1750.
- [118] D. Pathak, E. Shelhamer, J. Long, and T. Darrell, "Fully convolutional multi-class multiple instance learning," *arXiv preprint arXiv:1412.7144*, 2014.
- [119] D. Pathak, P. Krahenbuhl, and T. Darrell, "Constrained convolutional neural networks for weakly supervised segmentation," in *IEEE International Conference on Computer Vision*, 2015, pp. 1796–1804.

- [120] W. Shimoda and K. Yanai, "Distinct class-specific saliency maps for weakly supervised semantic segmentation," in *European Conference on Computer Vision*. Springer, 2016, pp. 218–234.
- [121] A. Kolesnikov and C. H. Lampert, "Seed, expand and constrain: Three principles for weakly-supervised image segmentation," in *European Conference on Computer Vision*. Springer, 2016, pp. 695–711.
- [122] P. O. Pinheiro and R. Collobert, "From image-level to pixel-level labeling with convolutional networks," in *IEEE Conference on Computer Vision and Pattern Recognition*, 2015, pp. 1713–1721.
- [123] S. Kwak, S. Hong, and B. Han, "Weakly supervised semantic segmentation using superpixel pooling network," in *AAAI Conference on Artificial Intelligence*, 2017.
- [124] J. Dai, K. He, and J. Sun, "BoxSup: Exploiting bounding boxes to supervise convolutional networks for semantic segmentation," in *IEEE International Conference on Computer Vision*, 2015, pp. 1635–1643.
- [125] D. Lin, J. Dai, J. Jia, K. He, and J. Sun, "ScribbleSup: Scribble-supervised convolutional networks for semantic segmentation," in *IEEE Conference on Computer Vision and Pattern Recognition*, 2016, pp. 3159–3167.
- [126] A. Bearman, O. Russakovsky, V. Ferrari, and L. Fei-Fei, "What's the point: Semantic segmentation with point supervision," in *European Conference on Computer Vision*. Springer, 2016, pp. 549–565.
- [127] S. Hong, H. Noh, and B. Han, "Decoupled deep neural network for semi-supervised semantic segmentation," in *Advances in neural information processing systems*, 2015, pp. 1495–1503.
- [128] A. Tarvainen and H. Valpola, "Mean teachers are better role models: Weight-averaged consistency targets improve semi-supervised deep learning results," in *Advances in neural information processing systems*, 2017, pp. 1195–1204.
- [129] T.-H. Vu, H. Jain, M. Bucher, M. Cord, and P. Pérez, "ADVENT: Adversarial entropy minimization for domain adaptation in semantic segmentation," in *IEEE Conference on Computer Vision and Pattern Recognition*, 2019, pp. 2517–2526.
- [130] Y. Zou, Z. Yu, B. Vijaya Kumar, and J. Wang, "Unsupervised domain adaptation for semantic segmentation via class-balanced self-training," in *European Conference on Computer Vision*, 2018, pp. 289–305.
- [131] A. Hu, A. Kendall, and R. Cipolla, "Learning a spatio-temporal embedding for video instance segmentation," *arXiv preprint arXiv:1912.08969*, 2019.
- [132] Y. He, W.-C. Chiu, M. Keuper, and M. Fritz, "Std2p: RGBD semantic segmentation using spatio-temporal data-driven pooling," in *IEEE Conference on Computer Vision and Pattern Recognition*, 2017, pp. 4837–4846.
- [133] D. Barnes, W. Maddern, and I. Posner, "Find your own way: Weakly-supervised segmentation of path proposals for urban autonomy," in *IEEE International Conference on Robotics and Automation*. IEEE, 2017, pp. 203–210.
- [134] T. Bruls, W. Maddern, A. A. Morye, and P. Newman, "Mark yourself: Road marking segmentation via weakly-supervised annotations from multimodal data," in *IEEE International Conference on Robotics and Automation*. IEEE, 2018, pp. 1863–1870.
- [135] X. Xu and G. H. Lee, "Weakly supervised semantic point cloud segmentation: Towards 10x fewer labels," in *IEEE Conference on Computer Vision and Pattern Recognition*, 2020, pp. 13 706–13 715.
- [136] J. Mei and H. Zhao, "Incorporating human domain knowledge in 3D LiDAR-based semantic segmentation," *IEEE Transactions on Intelligent Vehicles*, 2019.
- [137] K. Xu, Y. Yao, K. Murasaki, S. Ando, and A. Sagata, "Semantic segmentation of sparsely annotated 3D point clouds by pseudo-labelling," in *International Conference on 3D Vision*. IEEE, 2019, pp. 463–471.
- [138] D.-K. Kim, D. Maturana, M. Uenoyama, and S. Scherer, "Season-invariant semantic segmentation with a deep multimodal network," in *Field and Service Robotics*. Springer, 2018, pp. 255–270.
- [139] J. Mei, L. Zhang, Y. Wang, Z. Zhu, and H. Ding, "Joint margin, cograph, and label constraints for semisupervised scene parsing from point clouds," *IEEE Transactions on Geoscience and Remote Sensing*, vol. 56, no. 7, pp. 3800–3813, 2018.
- [140] M. Noroozi and P. Favaro, "Unsupervised learning of visual representations by solving jigsaw puzzles," in *European Conference on Computer Vision*. Springer, 2016, pp. 69–84.
- [141] C. Doersch, A. Gupta, and A. A. Efros, "Unsupervised visual representation learning by context prediction," in *IEEE International Conference on Computer Vision*, 2015, pp. 1422–1430.
- [142] D. Pathak, P. Krahenbuhl, J. Donahue, T. Darrell, and A. A. Efros, "Context encoders: Feature learning by inpainting," in *IEEE Conference on Computer Vision and Pattern Recognition*, 2016, pp. 2536–2544.
- [143] R. Zhang, P. Isola, and A. A. Efros, "Colorful image colorization," in *European Conference on Computer Vision*. Springer, 2016, pp. 649–666.
- [144] X. Wang and A. Gupta, "Unsupervised learning of visual representations using videos," in *IEEE International Conference on Computer Vision*, 2015, pp. 2794–2802.
- [145] D. Pathak, R. Girshick, P. Dollár, T. Darrell, and B. Hariharan, "Learning features by watching objects move," in *IEEE Conference on Computer Vision and Pattern Recognition*, 2017, pp. 2701–2710.
- [146] M. Noroozi, A. Vinjimoor, P. Favaro, and H. Pirsiavash, "Boosting self-supervised learning via knowledge transfer," in *IEEE Conference on Computer Vision and Pattern Recognition*, 2018, pp. 9359–9367.
- [147] J. Sauder and B. Sievers, "Self-supervised deep learning on point clouds by reconstructing space," in *Advances in Neural Information Processing Systems*, 2019, pp. 12942–12952.
- [148] A. Maligo and S. Lacroix, "Classification of outdoor 3D LiDAR data based on unsupervised gaussian mixture models," *IEEE Transactions on Automation Science and Engineering*, vol. 14, no. 1, pp. 5–16, 2016.
- [149] C. Tan, F. Sun, T. Kong, W. Zhang, C. Yang, and C. Liu, "A survey on deep transfer learning," in *Artificial Neural Networks and Machine Learning*, V. Kůrková, Y. Manolopoulos, B. Hammer, L. Iliadis, and I. Maglogiannis, Eds. Cham: Springer International Publishing, 2018, pp. 270–279.
- [150] Y. Ganin, E. Ustinova, H. Ajakan, P. Germain, H. Larochelle, F. Laviolette, M. Marchand, and V. Lempitsky, "Domain-adversarial training of neural networks," *The Journal of Machine Learning Research*, vol. 17, no. 1, pp. 2096–2030, 2016.
- [151] W. Dai, Q. Yang, G.-R. Xue, and Y. Yu, "Boosting for transfer learning," in *International Conference on Machine Learning*, 2007, pp. 193–200.
- [152] M. Long, Y. Cao, J. Wang, and M. Jordan, "Learning transferable features with deep adaptation networks," in *International Conference on Machine Learning*. PMLR, 2015, pp. 97–105.
- [153] M. Oquab, L. Bottou, I. Laptev, and J. Sivic, "Learning and transferring mid-level image representations using convolutional neural networks," in *IEEE Conference on Computer Vision and Pattern Recognition*, 2014, pp. 1717–1724.
- [154] S. Hong, J. Oh, H. Lee, and B. Han, "Learning transferrable knowledge for semantic segmentation with deep convolutional neural network," in *IEEE Conference on Computer Vision and Pattern Recognition*, 2016, pp. 3204–3212.
- [155] M. Abdou, M. Elkhateeb, I. Sobh, and A. Elsallab, "End-to-end 3D-pointcloud semantic segmentation for autonomous driving," *arXiv preprint arXiv:1906.10964*, 2019.
- [156] T. Roddick and R. Cipolla, "Predicting semantic map representations from images using pyramid occupancy networks," in *IEEE Conference on Computer Vision and Pattern Recognition*, 2020, pp. 11 138–11 147.
- [157] C. Lu, M. J. G. van de Molengraft, and G. Dubbelman, "Monocular semantic occupancy grid mapping with convolutional variational encoder-decoder networks," *IEEE Robotics and Automation Letters*, vol. 4, no. 2, pp. 445–452, 2019.
- [158] Ö. Er kent, C. Wolf, C. Laugier, D. S. González, and V. R. Cano, "Semantic grid estimation with a hybrid bayesian and deep neural network approach," in *IEEE/RSJ International Conference on Intelligent Robots and Systems*. IEEE, 2018, pp. 888–895.
- [159] J. Dequaire, P. Ondruška, D. Rao, D. Wang, and I. Posner, "Deep tracking in the wild: End-to-end tracking using recurrent neural networks," *The International Journal of Robotics Research*, vol. 37, no. 4-5, pp. 492–512, 2018.
- [160] M. Jaritz, T.-H. Vu, R. de Charette, É. Wirbel, and P. Pérez, "xMUDA: Cross-modal unsupervised domain adaptation for 3D semantic segmentation," *arXiv preprint arXiv:1911.12676*, 2019.
- [161] A. Shaban, S. Bansal, Z. Liu, I. Essa, and B. Boots, "One-shot learning for semantic segmentation," *arXiv preprint arXiv:1709.03410*, 2017.
- [162] C. Zhang, G. Lin, F. Liu, R. Yao, and C. Shen, "CANet: Class-agnostic segmentation networks with iterative refinement and attentive few-shot learning," in *IEEE Conference on Computer Vision and Pattern Recognition*, 2019, pp. 5217–5226.
- [163] J. Snell, K. Swersky, and R. Zemel, "Prototypical networks for few-shot learning," in *Advances in neural information processing systems*, 2017, pp. 4077–4087.
- [164] N. Dong and E. Xing, "Few-shot semantic segmentation with prototype learning," in *British Machine Vision Conference*, vol. 3, no. 4, 2018, p. 79.
- [165] P. Tian, Z. Wu, L. Qi, L. Wang, Y. Shi, and Y. Gao, "Differentiable meta-learning model for few-shot semantic segmentation," *arXiv preprint arXiv:1911.10371*, 2019.

- [166] F. Saleh, M. S. Aliakbarian, M. Salzmann, L. Petersson, S. Gould, and J. M. Alvarez, "Built-in foreground/background prior for weakly-supervised semantic segmentation," in *European Conference on Computer Vision*. Springer, 2016, pp. 413–432.
- [167] A. Kolesnikov and C. H. Lampert, "Improving weakly-supervised object localization by micro-annotation," *arXiv preprint arXiv:1605.05538*, 2016.
- [168] R. Mackowiak, P. Lenz, O. Ghorri, F. Diego, O. Lange, and C. Rother, "Cereals-cost-effective region-based active learning for semantic segmentation," *arXiv preprint arXiv:1810.09726*, 2018.
- [169] Z. Li, L. Zhang, R. Zhong, T. Fang, L. Zhang, and Z. Zhang, "Classification of urban point clouds: A robust supervised approach with automatically generating training data," *IEEE Journal of Selected Topics in Applied Earth Observations and Remote Sensing*, vol. 10, no. 3, pp. 1207–1220, 2016.
- [170] Z. Chen, Q. Liao, Z. Wang, Y. Liu, and M. Liu, "Image detector based automatic 3D data labeling and training for vehicle detection on point cloud," in *2019 IEEE Intelligent Vehicles Symposium*. IEEE, 2019, pp. 1408–1413.
- [171] F. Piewak, P. Pinggera, M. Schafer, D. Peter, B. Schwarz, N. Schneider, M. Enzweiler, D. Pfeiffer, and M. Zollner, "Boosting LiDAR-based semantic labeling by cross-modal training data generation," in *European Conference on Computer Vision*, 2018, pp. 0–0.
- [172] R. Varga, A. Costea, H. Florea, I. Giosan, and S. Nedevschi, "Supersensor for 360-degree environment perception: Point cloud segmentation using image features," in *IEEE International Conference on Intelligent Transportation Systems*. IEEE, 2017, pp. 1–8.
- [173] H. Luo, C. Wang, C. Wen, Z. Chen, D. Zai, Y. Yu, and J. Li, "Semantic labeling of mobile LiDAR point clouds via active learning and higher order MRF," *IEEE Transactions on Geoscience and Remote Sensing*, vol. 56, no. 7, pp. 3631–3644, 2018.
- [174] S. R. Richter, Z. Hayder, and V. Koltun, "Playing for benchmarks," in *IEEE International Conference on Computer Vision*, 2017, pp. 2213–2222.
- [175] P. Krähenbühl, "Free supervision from video games," in *IEEE Conference on Computer Vision and Pattern Recognition*, 2018, pp. 2955–2964.
- [176] G. Ros, L. Sellart, J. Materzynska, D. Vazquez, and A. M. Lopez, "The SYNTHIA dataset: A large collection of synthetic images for semantic segmentation of urban scenes," in *IEEE Conference on Computer Vision and Pattern Recognition*, 2016, pp. 3234–3243.
- [177] F. S. Saleh, M. S. Aliakbarian, M. Salzmann, L. Petersson, and J. M. Alvarez, "Effective use of synthetic data for urban scene semantic segmentation," in *European Conference on Computer Vision*. Springer, 2018, pp. 86–103.
- [178] J. K. Haas, "A history of the unity game engine," 2014.
- [179] F. Wang, Y. Zhuang, H. Gu, and H. Hu, "Automatic generation of synthetic LiDAR point clouds for 3-d data analysis," *IEEE Transactions on Instrumentation and Measurement*, vol. 68, no. 7, pp. 2671–2673, 2019.
- [180] A. Dosovitskiy, G. Ros, F. Codevilla, A. Lopez, and V. Koltun, "CARLA: An open urban driving simulator," *arXiv preprint arXiv:1711.03938*, 2017.
- [181] J. Fang, D. Zhou, F. Yan, T. Zhao, F. Zhang, Y. Ma, L. Wang, and R. Yang, "Augmented LiDAR simulator for autonomous driving," *IEEE Robotics and Automation Letters*, vol. 5, no. 2, pp. 1931–1938, 2020.
- [182] J. Fang, F. Yan, T. Zhao, F. Zhang, D. Zhou, R. Yang, Y. Ma, and L. Wang, "Simulating LiDAR point cloud for autonomous driving using real-world scenes and traffic flows," *arXiv preprint arXiv:1811.07112*, vol. 1, 2018.
- [183] A. Garcia-Garcia, S. Orts-Escolano, S. Oprea, V. Villena-Martinez, P. Martinez-Gonzalez, and J. Garcia-Rodriguez, "A survey on deep learning techniques for image and video semantic segmentation," *Applied Soft Computing*, vol. 70, pp. 41–65, 2018.
- [184] M. Bucher, T.-H. Vu, M. Cord, and P. Pérez, "Zero-shot semantic segmentation," *arXiv preprint arXiv:1906.00817*, 2019.
- [185] Y.-X. Wang, D. Ramanan, and M. Hebert, "Learning to model the tail," in *Advances in Neural Information Processing Systems*, 2017, pp. 7029–7039.
- [186] W. Zimmer, A. Rangesh, and M. Trivedi, "3D BAT: A Semi-Automatic, Web-based 3D annotation toolbox for full-surround, multi-modal data streams," *IEEE Intelligent Vehicles Symposium, Proceedings*, vol. 2019-June, pp. 1816–1821, 2019.
- [187] E. H. Lim and D. Suter, "3D terrestrial LiDAR classifications with super-voxels and multi-scale conditional random fields," *Computer-Aided Design*, vol. 41, no. 10, pp. 701 – 710, 2009.
- [188] H. Luo, C. Wang, C. Wen, Z. Chen, D. Zai, Y. Yu, and J. Li, "Semantic labeling of mobile LiDAR point clouds via active learning and higher order MRF," *IEEE Transactions on Geoscience and Remote Sensing*, vol. 56, no. 7, pp. 3631–3644, 2018.
- [189] C. Shorten and T. M. Khoshgofaar, "A survey on Image Data Augmentation for Deep Learning," *Journal of Big Data*, vol. 6, no. 1, 2019.
- [190] S. Cheng, Z. Leng, E. D. Cubuk, B. Zoph, C. Bai, J. Ngiam, Y. Song, B. Caine, V. Vasudevan, C. Li *et al.*, "Improving 3D object detection through progressive population based augmentation," *arXiv preprint arXiv:2004.00831*, 2020.
- [191] W. J. Scheirer, A. De Rezende Rocha, A. Sapkota, and T. E. Boult, "Toward open set recognition," *IEEE Transactions on Pattern Analysis and Machine Intelligence*, vol. 35, no. 7, pp. 1757–1772, 2013.
- [192] A. Khosla, T. Zhou, T. Malisiewicz, A. A. Efros, and A. Torralba, "Undoing the damage of dataset bias," in *European Conference on Computer Vision*. Springer, 2012, pp. 158–171.
- [193] T. Tommasi, N. Patricia, B. Caputo, and T. Tuytelaars, "A deeper look at dataset bias," in *Domain Adaptation in Computer Vision Applications*. Springer, 2017, pp. 37–55.



Biao Gao received B.S. degree in computer science (machine intelligence) from Peking University, Beijing, China, in 2017, where he is currently pursuing the Ph.D. degree with the Key Laboratory of Machine Perception (MOE), Peking University. His research interests include intelligent vehicles, 3D LiDAR perception, computer vision, and machine learning.



Yancheng Pan is currently pursuing the B.S. degree in computer science (machine intelligence) from Peking University, Beijing, China. He will continue pursuing the M.S. degree with the Key Laboratory of Machine Perception (MOE), Peking University. His research interests include computer vision, 3D LiDAR perception and intelligent vehicles.



Chengkun Li is currently pursuing the B.S. degree in Automation from Beijing Institute of Technology, Beijing, China. He is presently an intern student in the Key Laboratory of Machine Perception (MOE), Peking University. His research interests include computer vision, control and intelligent vehicles.



Sibo Geng is currently pursuing the B.S. degree in data science and big data from Yuanpei College, Peking University, Beijing, China. He is presently an intern student in the Key Laboratory of Machine Perception (MOE), Peking University, Beijing, China. His research interests include machine learning and intelligent vehicles.



Huijing Zhao received B.S. degree in computer science in 1991 from Peking University, China. From 1991 to 1994, she was recruited by Peking University in a project of developing a GIS platform. She obtained M.E. degree in 1996 and Ph.D. degree in 1999 in civil engineering from the University of Tokyo, Japan. After post-doctoral research as the same university, in 2003, she was promoted to be a visiting associate professor in Center for Spatial Information Science, the University of Tokyo, Japan. In 2007, she joined Peking Univ as an associate professor at the School of Electronics Engineering and Computer Science. Her research interest covers intelligent vehicle, machine perception and mobile robot.